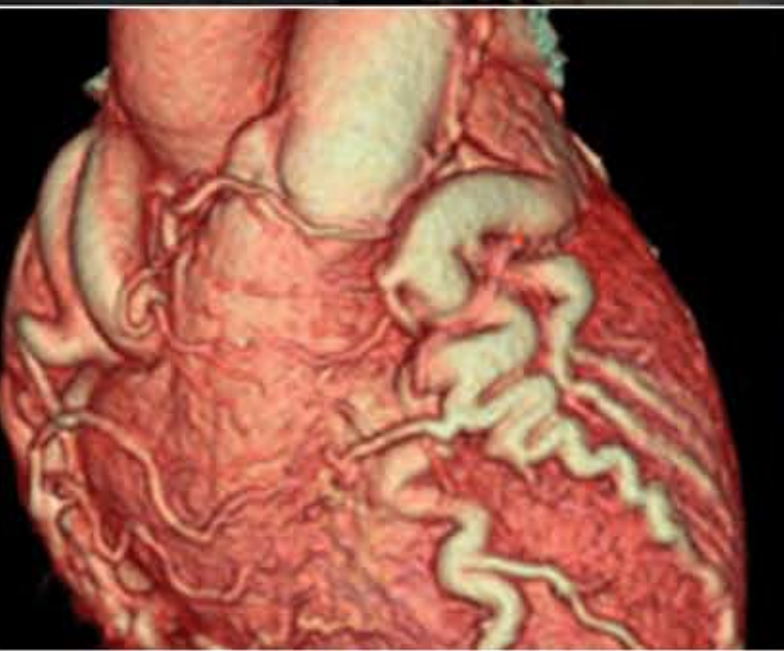


# COMPUTED TOMOGRAPHY OF THE CARDIOVASCULAR SYSTEM



THOMAS C. GERBER, M.D.  
BIRGIT KANTOR, M.D.  
ERIC E. WILLIAMSON, M.D.

# **Computed Tomography of the Cardiovascular System**



# Computed Tomography of the Cardiovascular System

*Edited by*

**Thomas C Gerber MD**

*Mayo Clinic, Jacksonville, FL, USA*

**Birgit Kantor MD**

*Mayo Clinic, Rochester, MN, USA*

**Eric E Williamson MD**

*Mayo Clinic, Rochester, MN, USA*

CRC Press  
Taylor & Francis Group  
6000 Broken Sound Parkway NW, Suite 300  
Boca Raton, FL 33487-2742

© 2007 by Taylor & Francis Group, LLC  
CRC Press is an imprint of Taylor & Francis Group, an Informa business

No claim to original U.S. Government works  
Version Date: 20141006

International Standard Book Number-13: 978-0-203-08974-3 (eBook - PDF)

This book contains information obtained from authentic and highly regarded sources. While all reasonable efforts have been made to publish reliable data and information, neither the author[s] nor the publisher can accept any legal responsibility or liability for any errors or omissions that may be made. The publishers wish to make clear that any views or opinions expressed in this book by individual editors, authors or contributors are personal to them and do not necessarily reflect the views/opinions of the publishers. The information or guidance contained in this book is intended for use by medical, scientific or health-care professionals and is provided strictly as a supplement to the medical or other professional's own judgement, their knowledge of the patient's medical history, relevant manufacturer's instructions and the appropriate best practice guidelines. Because of the rapid advances in medical science, any information or advice on dosages, procedures or diagnoses should be independently verified. The reader is strongly urged to consult the relevant national drug formulary and the drug companies' printed instructions, and their websites, before administering any of the drugs recommended in this book. This book does not indicate whether a particular treatment is appropriate or suitable for a particular individual. Ultimately it is the sole responsibility of the medical professional to make his or her own professional judgements, so as to advise and treat patients appropriately. The authors and publishers have also attempted to trace the copyright holders of all material reproduced in this publication and apologize to copyright holders if permission to publish in this form has not been obtained. If any copyright material has not been acknowledged please write and let us know so we may rectify in any future reprint.

Except as permitted under U.S. Copyright Law, no part of this book may be reprinted, reproduced, transmitted, or utilized in any form by any electronic, mechanical, or other means, now known or hereafter invented, including photocopying, microfilming, and recording, or in any information storage or retrieval system, without written permission from the publishers.

For permission to photocopy or use material electronically from this work, please access [www.copyright.com](http://www.copyright.com) (<http://www.copyright.com/>) or contact the Copyright Clearance Center, Inc. (CCC), 222 Rosewood Drive, Danvers, MA 01923, 978-750-8400. CCC is a not-for-profit organization that provides licenses and registration for a variety of users. For organizations that have been granted a photocopy license by the CCC, a separate system of payment has been arranged.

**Trademark Notice:** Product or corporate names may be trademarks or registered trademarks, and are used only for identification and explanation without intent to infringe.

Visit the Taylor & Francis Web site at  
<http://www.taylorandfrancis.com>

and the CRC Press Web site at  
<http://www.crcpress.com>

# Contents

---

<b>List of Contributors</b>	vii	11 Progression of Coronary Artery Calcium and its Pharmacologic Modification	143
<b>Foreword</b>	xi	<i>Axel Schmermund and Raimund Erbel</i>	
<b>Preface</b>	xiii	<b>Computed Tomographic Coronary Angiography</b>	
<b>Acknowledgments</b>	xv	12 How to Perform and Interpret Computed Tomography Coronary Angiography	155
<b>Introduction</b>		<i>Nico R Mollet, Niels Van Pelt, Willem B Meijboom, Annick Weustink, Francesca Pugliese, Filippo Cademartiri, Koen Nieman, Gabriel P Krestin, and Pim J de Feyter</i>	
1 History of Cardiovascular Computed Tomography	1	13 Computed Tomographic Angiography for the Detection of Coronary Artery Stenoses	163
<i>Martin J Lipton</i>		<i>Fabian Bamberg, Shawn DeWayne Teague, and Udo Hoffmann</i>	
2 Physics of and Approaches to Cardiovascular Computed Tomography	17	14 Computed Tomographic Angiography of Coronary Artery Anomalies	179
<i>Marc Kachelrieß</i>		<i>Phillip M Young, Ronald S Kuzo and Thomas C Gerber</i>	
3 Radiation Dose in Computed Tomography	27	15 Noninvasive Evaluation of Coronary Artery Bypass Grafts with Multislice Computed Tomography	193
<i>Michael F McNitt-Gray</i>		<i>Christof Burgstahler, Anja Reimann, Harald Brodoefel, Martin Heuschmid, Andreas F Kopp, and Stephen Schroeder</i>	
<b>Clinical Cardiovascular Computed Tomography</b>		16 Assessment of Coronary Artery Stents by Coronary Computed Tomographic Angiography	201
4 Cardiovascular Computed Tomography: A Clinical Perspective	39	<i>David Maintz and Harald Seifarth</i>	
<i>Mario J Garcia</i>		<b>Other Applications of Cardiac and Coronary Computed Tomography</b>	
5 Computed Tomographic Anatomy of the Heart	53	17 Computed Tomography of the Myocardium, Pericardium, and Cardiac Chambers	211
<i>Amgad N Makaryus and Lawrence M Boxt</i>		<i>James F Glockner</i>	
6 Pathology of Coronary Artery Atherosclerosis: Aspects Relevant to Cardiac Imaging	79	18 Assessment of Global and Regional Left Ventricular Function by Computed Tomography	229
<i>Dylan V Miller</i>		<i>Kai Uwe Juergens, Walter Heindel, and Roman Fischbach</i>	
7 Complementary Roles of Computed Tomography and Myocardial Perfusion Single Photon Emission Computed Tomography	89	19 Assessment of Heart Valve Disease by Computed Tomography	243
<i>Daniel S Berman, Leslee J Shaw, and Alan Rozanski</i>		<i>R van Lingen, N Manghat, C Roobottom, and G Morgan-Hughes</i>	
<b>Coronary Artery Calcium Scanning</b>			
8 Measurement of Coronary Artery Calcium by Computed Tomography	107		
<i>Thomas C Gerber, Christoph R Becker and Birgit Kantor</i>			
9 Coronary Calcium Scanning for the Prediction of Coronary Stenoses in Symptomatic Patients	119		
<i>Andreas Knez</i>			
10 Coronary Artery Calcification and Prediction of Major Adverse Cardiovascular Events	129		
<i>Leslee J Shaw, Paolo Raggi, Matthew J Budoff, and Daniel S Berman</i>			

20	Multislice Computed Tomography Evaluation of Congenital Heart Disease <i>Robert C Gilkeson, Kenneth G Zahka, and Ernest S Siwik</i>	261		
21	Computed Tomographic Imaging of the Cardiac and Pulmonary Veins: Role in Electrophysiology <i>Kalpathi L Venkatchalam and Peter A Brady</i>	273		
22	Extracardiac Findings on Cardiac Computed Tomographic Imaging <i>Karen M Horton and Elliot K Fishman</i>	291		
	<b>Peripheral Computed Tomographic Angiography</b>			
23	Computed Tomographic Angiography: Technical Considerations <i>Jacobo Kirsch, Eric E Williamson, and Dominik Fleischmann</i>	297		
24	Computed Tomographic Angiography of the Thoracic Aorta <i>Brad Thompson and Edwin J R van Beek</i>	307		
25	Computed Tomography for Pulmonary Embolism <i>Philip A Araoz</i>	321		
26	Computed Tomographic Angiography of the Abdominal Aorta and Iliac Arteries <i>Eric E Walser</i>	337		
27	Mesenteric and Renal Computed Tomographic Angiography <i>Fred M Moeslein, Eric E Williamson, and Dominik Fleischmann</i>	353		
28	Computed Tomographic Arteriography of the Upper and Lower Extremities <i>Jeffrey C Hellinger</i>	367		
29	Computed Tomographic Angiography of the Cervical Neurovasculature <i>Felix E Diehn and Paul Lindell</i>	391		
	<b>Investigational and Future Uses of Cardiovascular Computed Tomography</b>			
30	Cardiovascular Computed Tomography: A Research Perspective <i>Yue Dong and Erik L Ritman</i>	407		
31	Computed Tomographic Coronary Angiography for Subclinical Coronary Artery Disease, Coronary Artery Remodeling, and Plaque Imaging <i>Paul Schoenhagen</i>	417		
32	Imaging of Myocardial Viability and Infarction <i>Andreas H Mahnken and Arno Buecker</i>	429		
33	Computed Tomography for the Assessment of Myocardial Perfusion <i>Richard T George, Albert C Lardo, and Joao A C Lima</i>	441		
34	Dual-Energy Computed Tomography <i>Bernhard Schmidt and Cynthia McCollough</i>	451		
35	Hybrid Imaging Combining Cardiovascular Computed Tomography with Positron Emission Tomography <i>Roman Fischbach, Klaus Schäfers, and Kai Uwe Juergens</i>	463		
36	Full-Field Cardiac Imaging using Ultra-High Resolution Flat-Panel Volume-Computed Tomography <i>Rajiv Gupta, Soenke H Bartling, Mannudeep K Kalra, and Thomas J Brady</i>	473		
37	Micro Computed Tomography <i>Marc Kachelrieß</i>	491		
38	Imaging of Plaques and Vasa Vasorum with Micro-computed Tomography: Towards an Understanding of Unstable Plaque <i>Alexander C Langheinrich</i>	499		
	Index	509		

# Contributors

---

Philip A Araoz MD  
Mayo Clinic  
Rochester, MN, USA

Soenke H Bartling MD  
Molecular Imaging Junior Group  
German Cancer Research Center  
Heidelberg, Germany

Christoph Becker MD  
University Hospital Grosshadern  
Munich, Germany

Edwin JR van Beek MD  
Carver College of Medicine  
University of Iowa  
Iowa City, IA, USA

Daniel S Berman MD  
Cedars-Sinai Medical Center  
Los Angeles, CA, USA

Lawrence Boxt MD  
Manhasset, NY, USA

Peter A Brady MD  
Mayo Clinic  
Rochester, MN, USA

Thomas J Brady MD  
Massachusetts General Hospital  
Boston, MA, USA

Harald Brodoefel MD  
Eberhard-Karls-University Tuebingen  
Tuebingen, Germany

Arno Buecker MD  
University Hospital  
Hamburg, Germany

Matthew J Budoff MD  
Harbor-UCLA Medical Center  
Torrance, CA, USA

Christof Burgstahle MD  
Eberhard-Karls-University Tuebingen  
Tuebingen, Germany

Filippo Cademartiri MD PhD  
Erasmus Medical Center  
CA, Rotterdam, The Netherlands

Felix E Diehn MD  
Mayo Clinic  
Rochester, MN, USA

Yue Dong MD  
Mayo Clinic  
Rochester, MN, USA

Raimund Erbel MD  
West German Heart Center Essen  
University Essen-Duisburg  
Essen, Germany

Pim J de Feyter MD PhD  
Erasmus Medical Center  
CA, Rotterdam, The Netherlands

Roman Fischbach MD  
Department of Radiology  
Neuroradiology and Nuclear Medicine  
Asklepios Klinik Altona  
Hamburg, Germany

Elliot K Fishman MD  
Johns Hopkins Medical Institutions  
Baltimore, MD, USA

Mario Garcia MD  
Cleveland Clinic Foundation  
Cleveland, OH, USA

Richard T George MD  
Johns Hopkins Hospital  
Jefferson, Baltimore, MD, USA

Thomas C Gerber MD  
Mayo Clinic  
Jacksonville, FL, USA

Robert C Gilkeson MD  
University Hospitals of Cleveland  
CWRU Medical School  
Cleveland, OH, USA

James F Glocker MD  
Mayo Clinic  
Rochester, MN, USA

Rajiv Gupta PhD MD  
Massachusetts General Hospital  
Boston, MA, USA

Walter Heindel MD  
University of Muenster  
Muenster, Germany

Jeffrey C Hellinger MD  
The Children's Hospital of Philadelphia  
University of Philadelphia School of Medicine  
Philadelphia, PA, USA

Martin Heuschmid MD  
Eberhard-Karls-University Tuebingen  
Tuebingen, Germany

Udo Hoffmann MD  
Massachusetts General Hospital  
Harvard Medical School  
Boston, MA, USA

Karen M Horton MD  
Johns Hopkins Medical Institutions  
Baltimore, MD, USA

Kai Uwe Juergens MD  
Institut fur Klinische Radiologie  
Universitatsklinikum Munster  
Munster, Germany

Marc Kachelrieß MD PhD  
Institute of Medical Physics  
Friedrich-Alexander-University of Erlangen-Nurnberg  
Erlangen, Germany

Mannudeep K Kalra MD  
Massachusetts General Hospital  
Boston, MA, USA

Andreas Knez MD  
Medical Hospital  
Ludwig-Maximilians-University  
München, Germany

Andreas F Kopp MD  
Eberhard-Karls-University Tuebingen  
Tuebingen, Germany

Gabriel P Krestin MD PhD  
Erasmus Medical Center  
CA Rotterdam, The Netherlands

Ronald S Kuzo MD  
Mayo Clinic  
Jacksonville, FL, USA

Alexander C Langheinrich MD  
Justus-Liebig-University  
Giessen, Germany

Albert C Lardo PhD  
Johns Hopkins Hospital  
Jefferson, Baltimore, MD, USA

Joao A C Lima MD  
Johns Hopkins Hospital  
Jefferson Baltimore, MD, USA

Paul Lindell MD  
Mayo Clinic  
Rochester, MN, USA

Andreas H Mahnken MD MBA  
University Hospital  
RWTH Aachen University  
Aachen, Germany

Martin Lipton MD  
Sausalito, CA, USA

David Maintz MD  
University of Muenster  
Munster, Germany

Amgad N Makaryus MD  
Columbia University School of Medicine  
New York, NY, USA

Cynthia McCollough MD  
Mayo Clinic College of Medicine  
Rochester, MN, USA

Michael McNitt-Gray MD  
David Geffen School of Medicine, UCLA  
Los Angeles, CA, USA

Willem B Meijboom MD  
Erasmus Medical Center  
CA Rotterdam, The Netherlands

Dylan V Miller MD  
Mayo Clinic  
Rochester, MN, USA

Nico R Mollet MD PhD  
Erasmus Medical Center  
CA Rotterdam, The Netherlands

Gareth Morgan-Hughes MD  
Plymouth NHS Trust  
Plymouth, United Kingdom

Fabian Bamberg MD  
Massachusetts General Hospital  
Harvard Medical School  
Boston, MA, USA

Koen Nieman MD PhD  
Erasmus Medical Center  
CA Rotterdam, The Netherlands

Niels Van Pelt MD  
Erasmus Medical Center  
CA Rotterdam, The Netherlands

Paolo Raggi MD  
Emory University School of Medicine  
Atlanta, GA, USA

Anja Reimann MD  
Eberhard-Karls-University Tuebingen  
Tuebingen, Germany

Erik L Ritman MD  
Mayo Clinic  
Rochester, MN, USA

Alan Rozanski MD  
St. Luke's Roosevelt Hospital Center  
New York NY, USA

Klaus Schäfers MD  
Institut für Klinische Radiologie  
Universitätsklinikum Munster  
Munster, Germany

Axel Schmermund PhD  
Cardioangiologisches Centrum Bethanien  
Frankfurt, Germany

Bernhard Schmidt MD  
Siemens Medical Solutions  
Forchheim, Germany

Paul Schoenhagen MD FAHA  
Cleveland Clinic Foundation  
Cleveland, OH, USA

Stephen Schroeder MD  
Eberhard-Karls-University Tuebingen  
Tuebingen, Germany

Leslee J Shaw PhD  
Emory University School of Medicine  
Atlanta, GA, USA

Ernest S Siwik MD  
University Hospitals of Cleveland  
CWRU Medical School  
Cleveland, OH, USA

Shawn DeWayne Teague MD  
Indiana University Hospital  
Indianapolis, IN, USA

Brad Thompson MD  
Carver College of Medicine  
University of Iowa, Iowa City, IA, USA

Kalpathi L Venkatachalam  
Mayo Clinic  
Rochester, MN, USA

Eric E Walser MD  
Mayo Clinic  
Jacksonville, FL, USA

Annick Weustink MD  
Erasmus Medical Center  
CA Rotterdam, The Netherlands

Erik E Williamson MD  
Mayo Clinic  
Rochester, MN, USA

Phillip Young MD  
Mayo Clinic  
Jacksonville, FL, USA

Kenneth G Zahka MD  
University Hospitals of Cleveland  
CWRU Medical School  
Cleveland, OH, USA



# Foreword

---

The use and acceptance of computed tomography (CT) in the clinical workup of patients with known or suspected cardiovascular disease is increasing rapidly. In particular, coronary CT angiography has become robust and accurate within the last few years. With CT technology evolving rapidly, coronary CT angiography has developed from the stage of “proof of principle” into a stable imaging modality that is clinically useful for many patients. All the same, uncertainties remain, and in order to use coronary CT angiography in the clinically most useful manner, detailed knowledge of its potential and limitations is required.

As more and more clinicians are considering the use of cardiovascular CT in their clinical practice, and as more and more researchers contribute to the evidence base for the use of this technology, students and users of cardiovascular CT must assimilate a large amount of information. Since the advantages and limitations of CT in clinical practice are closely related to how the images are generated, a solid understanding of the technical principles underlying cardiovascular CT is essential. Knowledge of cardiac anatomy needs be revisited from the perspective of cross-sectional and three-dimensional imaging. Practitioners of cardiovascular CT must understand imaging protocols and algorithms in detail to be able to adapt them to individual clinical questions. The usefulness and accuracy of CT imaging for a wide range of diagnostic problems in cardiovascular disease needs to be understood and finally, with the field of cardiovascular CT moving forward rapidly, one should

have an idea of what the near future holds in terms of technological developments and new clinical applications.

The magnificent book *Computed Tomography of the Cardiovascular System*, edited by Drs Gerber, Kantor and Williamson effortlessly covers this wide range of information and addresses all relevant areas with contributions from renowned experts in the field. This book is a rich source of information for both new and experienced users of cardiovascular CT and successfully puts current and future applications into technical and clinical context. The editors are to be commended for providing the medical community with such a complete but very readable account at a time when the need for reliable and concise yet thorough information is immense.

I congratulate Drs. Gerber, Kantor, and Williamson, along with their authors, for bringing this book to life. Without a doubt it will be a tremendously important resource to healthcare providers who order, perform or interpret cardiovascular CT studies and who must understand which patients and clinical scenarios benefit most from its use. As such, the book will be not only a wonderful and lasting reference but, because of its balanced approach to cardiovascular CT, will also make an important contribution to the rational growth of this field.

**Stephan Achenbach MD**  
Professor of Medicine  
University of Erlangen  
Erlangen, Germany



# Preface

---

This book is a labor of love by imaging enthusiasts from all over the world, meant for individuals interested in mastering cardiovascular computed tomography (CT). Two ideas have guided the development of its content: 1. both cardiologists and radiologists can become expert readers of cardiovascular CT studies and 2. the cardiovascular system is not separated at the aortic valve into two entirely disparate parts. To emphasize these points, we have invited cardiologists as well as radiologists as contributors, and have included a large section on vascular radiology which is missing from most current textbooks on cardiac CT.

Cardiovascular CT in its current, widely embraced form is a relatively young field. As a result, the evidence base for its use is still being developed, and there is controversy about the appropriateness of cardiovascular CT imaging in specific clinical situations. To address such concerns, we have included chapters on clinical context and on the relationship between CT and more established cardiovascular imaging techniques. Cardiovascular CT is evolving rapidly, and in order to avoid publishing material that is obsolete by the time it appears in print, we have placed great emphasis on discussing principles that are as much as possible independent of type and generation of CT scanners.

We have organized the book to progress from a discussion of basic concepts in cardiovascular CT, over descriptions of a wide array of clinical applications, to uses of CT that are currently considered investigational but are clearly on the horizon for the clinical realm and that contribute to the understanding of clinical problems in cardiology. Placing chapters on general issues next to chapters on specific aspects of cardiovascular CT has created minor overlaps that are intentional and that allow each chapter in the book to stand alone and be easily read and understood by itself.

We are very proud of, and grateful to, the many experts in CT from the U.S. and from abroad who have generously agreed to devote their time to contributing articles and who have made this book a unique and complete account of the current status of cardiac, vascular, and investigational applications of cardiovascular CT. We trust that readers will find it a valuable resource as they study the clinical use and the future potential of cardiovascular CT.

Thomas C Gerber  
Birgit Kantor  
Eric E Williamson



# Acknowledgments

---

For Freya and Maximilian, who teach us as much about being good as we are teaching them.  
B.K. and T.C.G.

To my parents, Eva and Hermann Gerber, in deep gratitude.  
T.C.G.

To Geoff Rubin, Dominik Fleischmann and Jerry Breen who continue to teach me about cardiovascular CT. To Mary Jo who has supported me in every way possible, and to Alex and Katherine – the most fascinating people I know.  
E.E.W



# History of Cardiovascular Computed Tomography

---

Martin J. Lipton

## I INTRODUCTION

Historically, the diagnosis of heart disease has depended largely upon radiographic methods. This chapter describes the key requirements for imaging the heart using conventional X-ray methods and with Computed Tomography (CT) when it became available; it describes the feasibility and validation studies which formed the basis for modern clinical cardiac CT.

## 2 X-RAY IMAGING FROM 1895–1972 – PRE-CT ERA

The discovery of X-rays by W. Conrad Roentgen in 1895 had a dramatic and immediate impact in two fields. Not only did it create a new medical specialty called Roentgenology, named in honor of its founder, but also it profoundly changed the thinking of physicists of that time regarding the nature of atomic structure. Industry became heavily involved in the X-ray field from the beginning, because high vacuum tubes and more powerful generators were essential for the production of X-rays. Progressive improvements also occurred in all aspects of X-ray imaging, which became a big business driven by the diagnostic needs of physicians.<sup>1</sup>

Diseases of the heart and blood vessels represent one of the most challenging problems for advanced diagnostic

imaging systems. The history of radiographic diagnosis over the decades following Roentgen's discovery explain to some extent the philosophic and practical differences between cardiology and radiology. Radiologists are traditionally trained to observe and recognize the broad range of normal anatomy and pathology. Since diagnostic imaging of most organs relies primarily on structural findings, industry responded by providing higher spatial and contrast resolution. Cardiologists, however, are primarily concerned with cardiac function, and use imaging methods routinely to quantitate cardiac indices. This explains why dedicated and specialized equipment with high temporal resolution is necessary for every modality for cardiac imaging. Cardiac catheterization with haemodynamic recording and angiocardiology emerged as the most useful and reliable technique for evaluating patients prior to cardiac surgery. This generally has remained the practice despite remarkable advances in the established noninvasive fields of echocardiography and nuclear medicine. Cine-angiocardiology provides high temporal resolution in excess of 30 images per second without the need for ECG-gating. It does, however, require selective catheterization and contrast media injections. All conventional X-ray projection imaging methods suffer from the limitation of overlapping structures and, therefore, multiple angiographic projections are necessary, each of which requires an additional injection of contrast media. Nevertheless, invasive angiocardiology became established as the gold standard for identifying the





**Figure 1.2** A localizing slice level through the heart in a patient.

Firstly, it is impossible to display within the framework of a two-dimensional X-ray, a three-dimensional scene under view. Objects situated in depth, i.e. in the third dimension, superimpose, causing confusion to the viewer.

Secondly, conventional X-ray cannot distinguish between soft tissues. In general, a radiogram differentiates only between bone and air, as in the lungs. Variation in soft tissues such as the liver and pancreas are not discernible at all and certain other organs may be rendered visible only through the use of radio-opaque dyes.

Thirdly, when conventional X-ray methods are used, it is not possible to measure in a quantitative way the separate densities of the individual substances through which the X-ray has passed. The radiogram records the mean absorption by all the various tissues which the X-ray has penetrated. This is of little use for quantitative measurement.

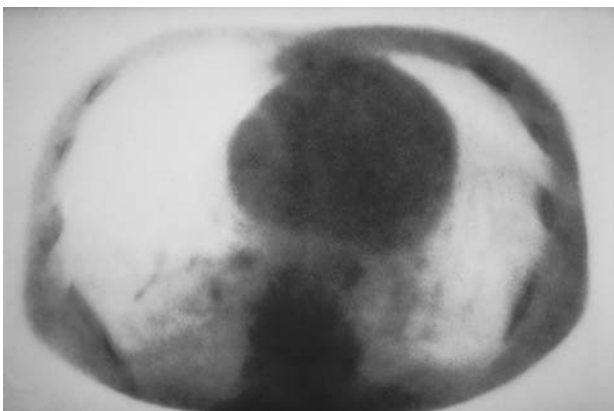


**Figure 1.3** An example of the image obtained by axial tomography. Note that this blurring is due to simple back projection radiography and although quite useful has limitations.

**Table 1.1** Development of computed tomography

Year	Development	Inventor
1947	Axial tomography (AT)	Takahashi
1964 to 1966	Computed tomography	*Cormack /Kuhl
1972	First fan beam scanner	Boyd
1972	First commercial scanner	*Hounsfield
1973	5 minute CT scanner	
1976	20 second EMI scanner	
1977	5 second body scanner	
1978	Proposed cardiac scanners	
	**DSR	Ritman
	+CVCT	Boyd
	++EB CT	

\*Nobel prize 1979.  
 \*\*Dynamic Spatial Reconstructor (DSR)  
 +CVCT = cine computed tomographic C-100 scanner or  
 ++Electron Beam (EB CT)

Computed tomography, on the other hand, measures the attenuation of X-ray beams passing through sections of the body from hundreds of different angles, and then, from the evidence of these measurements, a computer is able to reconstruct pictures of the body's interior.

Pictures are based on the separate examination of a series of contiguous cross sections, as though we looked at the body separated into a series of thin 'slices.' By doing so, we virtually obtain total three-dimensional information about the body.<sup>23</sup>

The era of digital imaging began with CT, and has since been applied to many other imaging modalities. CT has a density range of 2,000 shades of gray. The human eye can only recognize 11–21 approximately. Because the sensitivity of CT for density is over 1% and so much more sensitive than conventional X-ray film combinations, intravenous enhancement of the blood volume, combined with cross sectional imaging, provides sufficient contrast for angiography and avoids the need for arterial injections.

Early studies of CT for cardiovascular imaging explore the capability of CT to overcome the 3 major limitations of conventional X-ray. However, CT cannot yet match the resolution of conventional X-ray imaging, nor its exposure speed, or cost. However, as CT develops it will no doubt eventually replace almost all types of X-ray imaging.

The first CT scanners required 1–5 seconds to acquire a single slice. However, this was adequate for diagnosing most organ systems, because temporal resolution was not critical. These machines were designed initially for the head, and later for whole body. The impact of this new

modality was dramatic, for example in neuroradiology the need for invasive angiography fell by almost 50%, and CT virtually replaced diagnostic nuclear scintigraphy in the brain. As Godfrey Housfield implied, within a few years CT dominated head imaging. Early CT studies of the heart however were confined to exploring morphology.<sup>4-7</sup>

## 5 CT ESTIMATES OF VENTRICULAR VOLUMES, WALL THICKNESS AND MASS

A critical measurement for evaluating cardiac function is left ventricular ejection fraction. Biplane angiography provided the most accurate and reproducible results.<sup>8</sup> One of the first cardiac quantitative studies explored the capability of CT for accurate volume measurements of postmortem silastic casts of the human left ventricle. The effect of cast shape and orientation on volume measurements was evaluated. Results were compared with those obtained by biplane radiography and by Archimedes principle.<sup>9</sup> Cast angulation was precisely measured for each technique, as illustrated in Figures 1.4 and 1.5. The true cast volume for validation was obtained for each cast using a Mettler balance to measure dry cast weight in air, and a torsion balance for each cast submerged in distilled water. Air trapped in the casts while submerged between trabecular and papillary muscles which can cause significant errors, was eliminated by degassing under water. The results are given in Figures 1.6 and 1.7 and were calculated by dividing the difference between the dry and submerged weight of each cast by the density of water at a recorded temperature. This study demonstrated

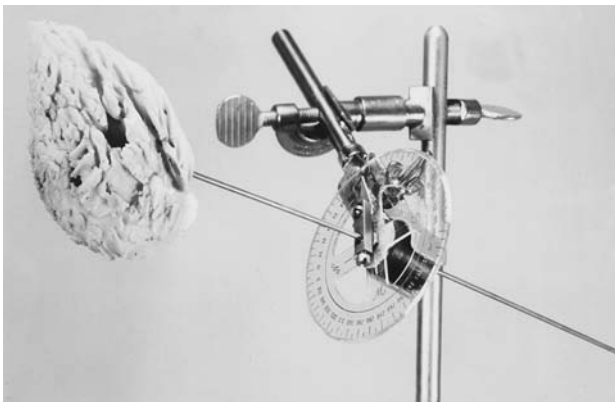


**Figure 1.4** Ventricular cast in a stand which allows it to be positioned in any orientation for biplane volume measurement. (From ref. 10 with permission)

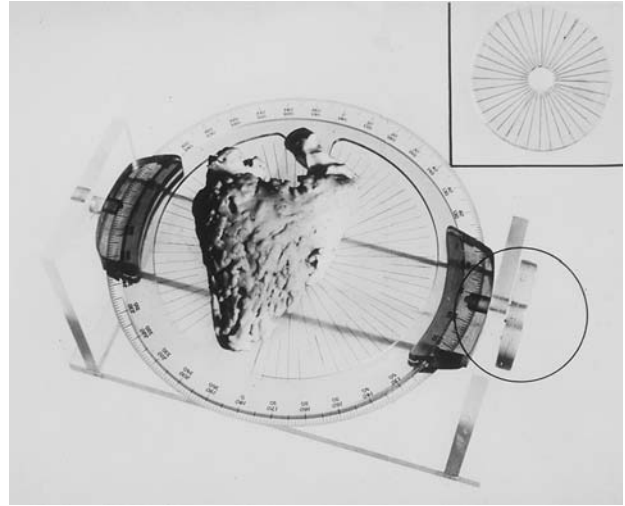


**Figure 1.5** Casts were placed on a Plexiglas goniometer, which enables precise cast orientation in three planes insuring accurate positioning for computed tomographic volume measurements. Plexiglas does not interfere with computed tomographic reconstruction. (From ref. 10 with permission)

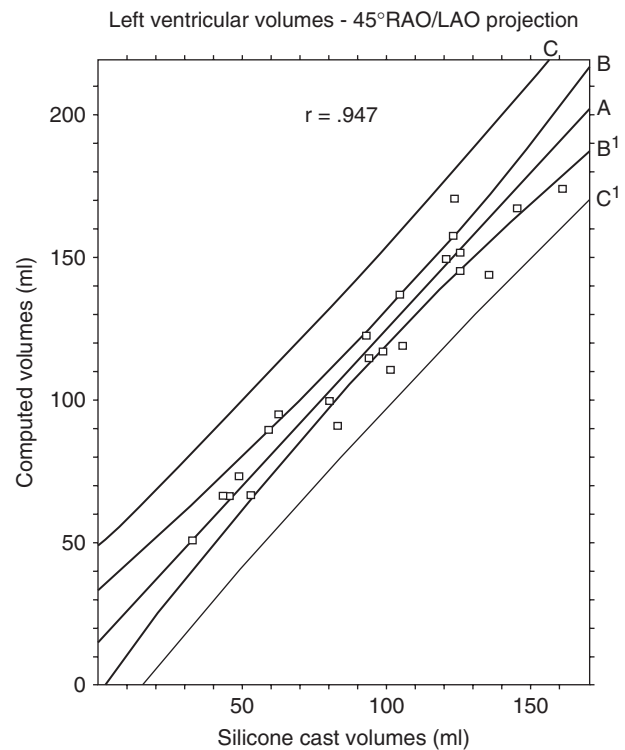


**Figure 1.6** Left ventricular volumes measured by radiography in the anteroposterior-lateral projections plotted against actual cast volumes. Ninety-five percent confidence limits for the regression lines are indicated by line BB', and 95% confidence limits for individual measurements are indicated by lines CC'. (From ref. 10 with permission)

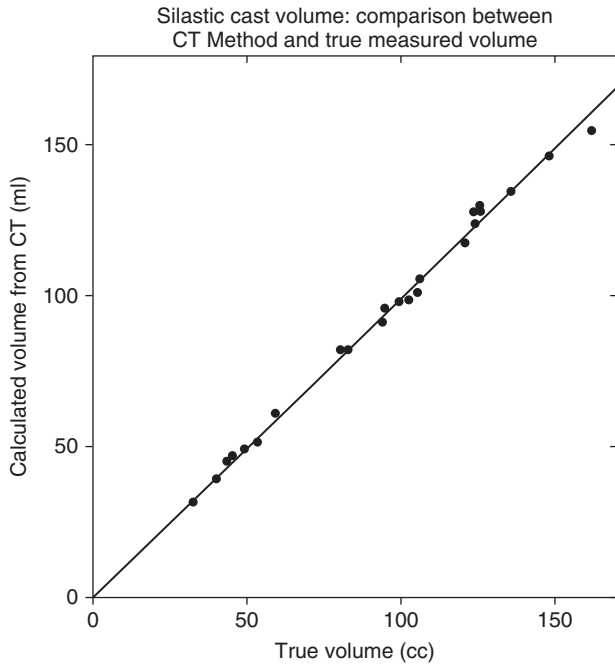


**Figure 1.7** Calculated computed tomographic volumes plotted against true cast volumes. The regression line practically coincides with the line of identity. The correlation coefficient is 0.998. (From ref. 10 with permission)

the superiority of cross sectional 3-dimensional CT of the heart and raised several issues which are generic, including methods for edge detection, the influence on accuracy of CT windowing and level and the question of how many axial images and therefore slices are required to provide precise volume estimates for a given cardiac chamber. It also became apparent that, for each type of new scanner, such calibration issues would need to be addressed.<sup>10,11</sup>

## 6 MYOCARDIAL WALL DIMENSIONS AND MASS

The potential of CT for quantitative assessment of inter-ventricular septal wall thickness was evaluated *in vivo* in dogs. Fourteen pedigree beagle puppies of both sexes comprised this study population. Seven underwent aortic banding at 6–8 weeks, so that the supravalve aortic circumference was reduced 25–40%. All the dogs were followed and scanned at 7–9 months. The study was performed using a General Electric CT/T 7800 Research Scanner (modified GE whole body scanner). This unit could perform rapid sequential scanning, acquiring up to 12, 360° scans in 40 seconds; each having a 2.4 second exposure time.

This scanner was among the first to produce a projection ‘scout view’ or computed radiograph by pulsing the X-ray tube with the detector array in a stationary position, while the subject is moved through the X-ray field. The lateral scout view was used in this study to locate the cardiac apex, and all subsequent scans were indexed to this reference level, which was precisely identified under computer/operator control. Until this view became available, surface landmarks had to be used and scanning levels could not be reliably reproduced. Today such localizing aids with lasers are taken for granted, and universally supplied with every CT scanner. Figure 1.8 illustrates one typical pair of CT scans from this study, and demonstrated the marked left ventricular hypertrophy compared with a litter matched control. A linear regression line for septal wall thickness was obtained by plotting the CT estimates derived from regions of interest (ROI), like the one seen in Figure 1.8, which includes both ventricles, against direct autopsy measurements, as shown in Figure 1.9. The correlation coefficient was 0.92 for the 14 experiments. Non-ECG-gated CT underestimated the autopsy values by 10–20%. However, this was a consistent underestimation. At that time, a paper pixel print out map had to be obtained of the ROI, as shown in Figure 1.10. Edge detection is critical for measurements. A boundary CT number was defined as the CT number halfway between the mean CT number of the ventricular cavities and the midpoint of the septal wall, from which the mean width is calculated.<sup>12</sup>

A study of left ventricular mass using 22 dogs and the same scanner was also performed. This research scanner was installed in UCSF in 1977 and was continuously modified for cardiac applications. The gantry of this single slice machine, like all early CT scanners, had to be rotated in opposite directions between scan sequences, since the power cables would twist, limiting rotation and resulting in long interscan delay times. The CT data analysis involved two methods, a semi-automated computer technique and a manual tracing technique to define the myocardial boundary. Both methods showed similar results<sup>13</sup> (Figure 1.11). Such non ECG-gated CT feasibility studies are logical necessary steps in developing new clinical tools. However, extrapolating results to patients must be guarded. Nevertheless, this study showed that CT provides accurate dimensional measurements. Furthermore, in the presence of asymmetrical hypertrophy or abnormal chamber configurations or both, CT, unlike echocardiography, should be superior, because no geometric assumptions are necessary later, Feiring measured LV mass by EBCT concerning its accuracy and precision.

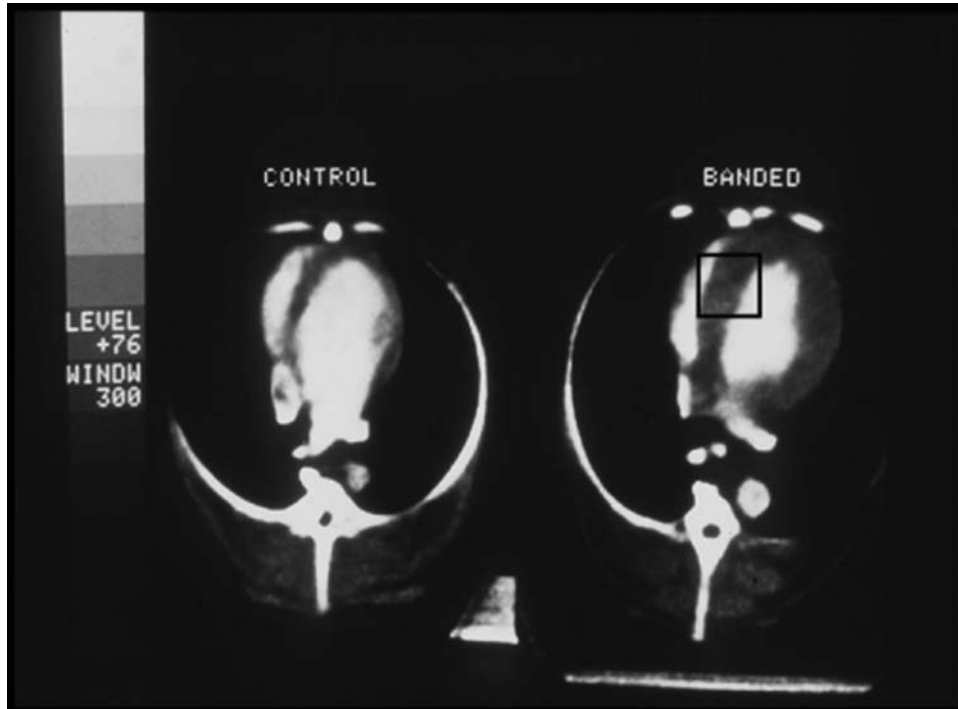


**Figure 1.8** (a) Nongated, 1-cm thick computed transmission tomographic scan through the ventricular cavities of a non-banded control beagle after intravenous injection of contrast medium. (b) A similar scan at the same level is seen in a matched litter mate 7 months after banding. The myocardial wall is symmetrically hypertrophied and the relatively smaller contrast-enhanced left ventricular cavity is apparent. A region of interest has been selected to include a portion of both the right and left ventricular cavities.

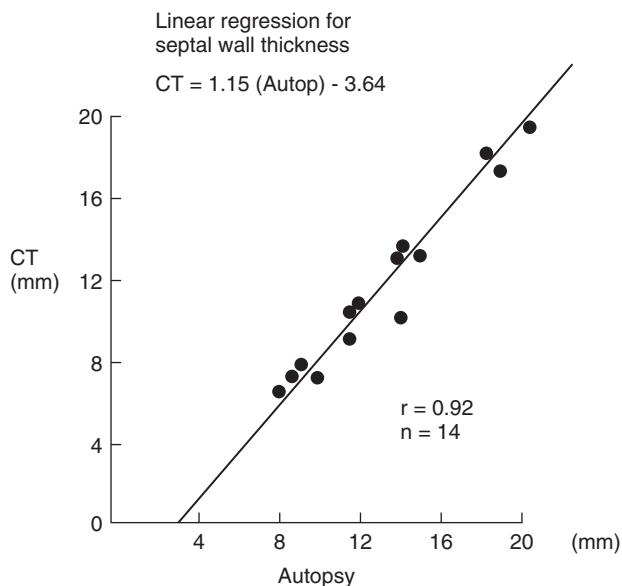


**Figure 1.9** Linear regression for septal wall thickness; along the abscissa are measurements (mm) obtained at autopsy and corresponding computed transmission tomographic estimates lie on the ordinate. (From ref. 12 with permission)

## 7 ECG-GATED COMPUTED TOMOGRAPHIC

An exciting prospect for CT is quantitation of cardiac chamber and myocardial wall thickening dynamics for which ECG-gated CT was explored in a number of centers with single slice scanners in 1979 and 1980s.<sup>14-18</sup> This technique is one method of overcoming the problem of cardiac motion and is critical in obtaining quantitative dimensional data, ejection fractions and also for measuring the extent of wall thickening during the cardiac cycle.

Gated CT differs significantly from standard computed tomographic scanning. It was well realized 25 years ago that to obtain a reconstructed image of a stationary object by standard computed tomography, a full complement of angular X-ray data must be obtained over the full scanning circle from 0 to 360° without significant gaps in the angular data set, although some gating programs use only 180° plus the fan beam angle. However, no gaps are permitted in this data.

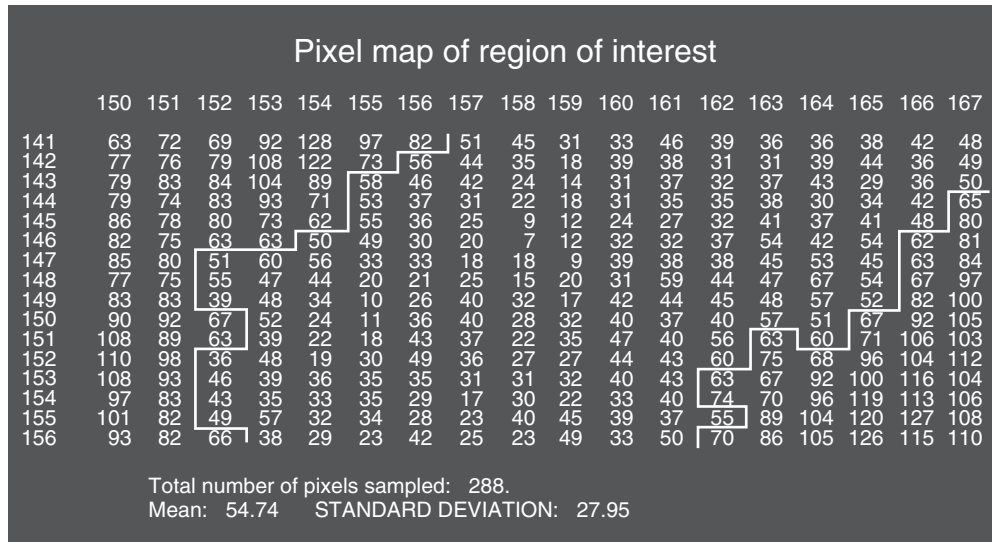


**Figure 1.10** Computer printout of absolute computed transmission tomographic (CT) numbers present within the same region of interest as described in Figure 1.8. Each pixel is  $1.3 \times 1.3$  mm. Lines demarcate all pixels with absolute CT numbers of 60 or less, thus defining the interventricular septum. This boundary CT number was defined as the CT number that was halfway between the mean CT number of the cavities and the mean CT number of the midportion of the septal wall. Scale drawing of the septum then defined the septal boundary within the region of interest, from which the mean width is calculated.

Therefore, multiple scans are required to obtain the necessary angular data to reconstruct a gated image of the heart.

## 8 RETROSPECTIVE VERSUS PROSPECTIVE GATING

Two gating techniques were utilized: retrospective<sup>19</sup> and prospective<sup>18</sup> gating. With retrospective gating, the computed tomographic scan data and the electrocardiogram are simultaneously recorded, and the CT data is binned to correspond with selected ECG windows. The prospective gating system allowed preselection of a fraction of the electrocardiographic RR interval width to be monitored.<sup>18</sup> The biologic window width sets the fraction of the cardiac cycle to be represented by each image. Prospective gating assures the even distribution of the R waves throughout the scanning circle in the minimal number of scans. This is accomplished by launching the X-ray tube at the appropriate time relative to the R wave on the electrocardiographic input, such that one of the following R waves falls in the largest gap in the already acquired angular X-ray data. In our studies, the width of the biologic window was set at 10% of the RR interval. Since the heart rate was maintained between 100 and 120 beats/min in dogs, each frame represents 0.05 to 0.06 second. With the biologic window set at 10% of the RR interval, approximately eight scans were

Measurement of LV mass by CT (computer method)

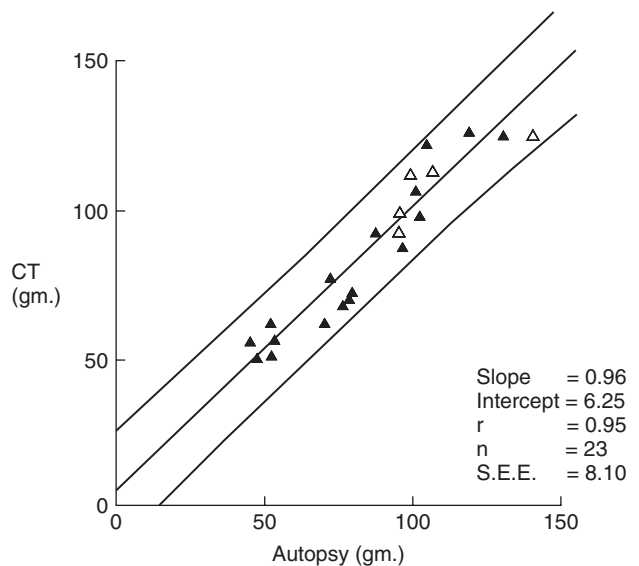


**Figure 1.11** Relation between autopsy values and computed tomographic (CT) estimates of left ventricular (LV) mass. Results for the computer method. Filled triangles represent normotensive dogs; open triangles represent the beagles with left ventricular hypertrophy. The lines on either side of the regression line indicate the 95 percent confidence limits. (From ref. 13 with permission)

**Table 1.2** Limitations of whole body scanners in 1980s

- 1) Exposure time is too long (1 to 5 seconds).
- 2) Repetition rate is too slow (0.5 to 2 second delay).
- 3) Single slice capability.
- 4) Heat load limitations of X-ray tube severely restricts the number of scans in dynamic sequence.
- 5) EKG gating is cumbersome.
- 6) Breath holding requirements are excessive for gating.
- 7) Requires relatively large volumes of contrast medium.
- 8) Quantitation of many functions is limited.

required to obtain a full complement of ECG-gated angular data, requiring approximately 45 seconds of breath-holding. The limitations of CT during this early period are summarized in Table 1.2.

## 9 CT EVALUATION OF MYOCARDIAL ISCHEMIA AND INFARCTION

Early CT studies of acute myocardial infarction (AMI) were performed in several centers on ex situ or arrested dog hearts.<sup>4-7</sup> The group at UCSF explored the detection and quantitation of myocardial injury in vivo using intracoronary and intravenous contrast media.<sup>20-21</sup> While the attenuation of infarcted myocardium was less than normal tissue and could be detected, it was much easier to identify with contrast enhancement.

## 10 CONTRAST ENHANCEMENT OF ACUTE MYOCARDIAL INFARCTION

Contrast material produces temporally distinct phases of enhancement of normal and ischemically damaged myocardium. During the perfusion phase, normal myocardium is maximally enhanced (maximum increase in X-ray attenuation value), whereas the area of damage is nonenhanced or minimally enhanced (Figure 1.12). Ten minutes after administration of the contrast material, enhancement of normal myocardium has declined and the damaged myocardium is nearly maximally enhanced. In the perfusion phase, the ischemically damaged area appears as a 'negative image' within the myocardium, whereas in the

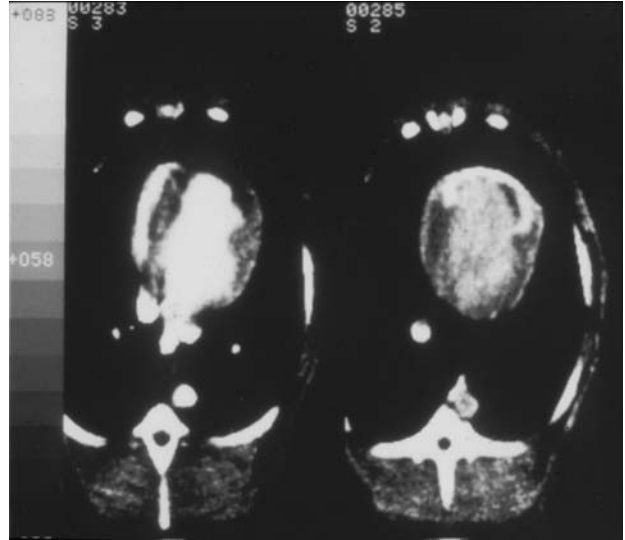


**Figure 1.12** Two contrast enhanced CT scans acquired with a conventional whole body single slice scanner at the same level in a dog with an acute myocardial infarction in the antero-septal wall. The left image is during the first pass of an intravenous bolus of contrast agent. Note the myocardial enhancement void in the infarct area. The image on the right was obtained 10 minutes later after contrast washout has occurred. The infarct zone is seen as a bright, horseshoe area of delayed enhancement.

later phase, it appears as a 'positive image.' The early CT appearances reflect reduced tissue perfusion, while later, after more prolonged occlusion, it was thought to be related to necrosis and scar formation. Both iodinated contrast material and <sup>99m</sup>Tc-pyrophosphate were shown to be markers of myocardial necrosis. In some infarcts, both substances had a high concentration within the center, periphery, and margin of the infarct, whereas in others, the concentration of both substances was low in the center and high in the periphery and margin of the infarct. Measurement of regional myocardial blood flow with indium-111-labeled microspheres indicated that the accumulation of both contrast material and <sup>99m</sup>Tc-pyrophosphate in the center of the infarct occurred when residual blood flow was at least 3% of normal myocardial blood flow. Neither substance accumulates in the region of infarcted myocardium with a residual blood flow of less than 3% of normal. These studies inferred that contrast enhancement of ischemically damaged tissue is a marker of myocardial necrosis, but its occurrence is dependent upon the presence of a threshold level of residual myocardial perfusion.<sup>22-24</sup>

Doherty et al. performed an vivo AMI study with 28 dogs and showed that the distribution of contrast enhancement was not only similar to technetium-<sup>99m</sup>

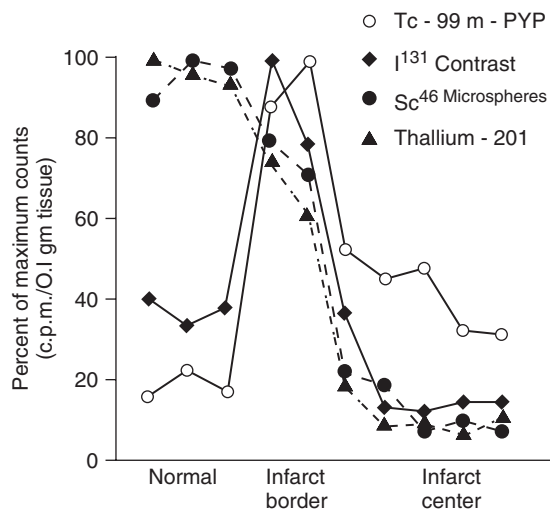
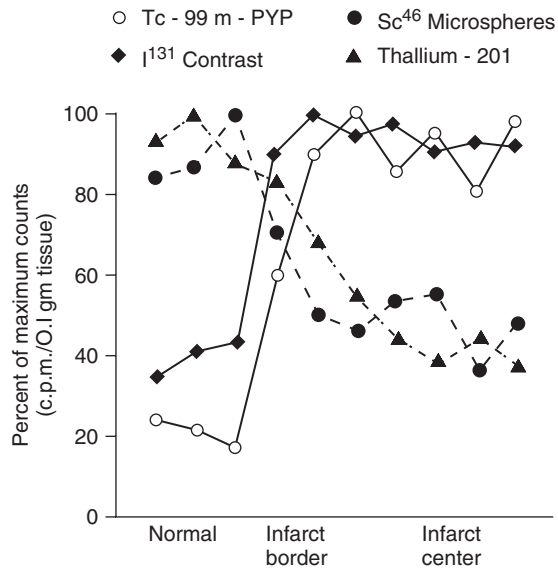


**Figure 1.13** Distribution of pyrophosphate, thallium, microspheres and contrast material in (A) epicardial and (B) endocardial samples for a representative transmural anterior infarct. (A) The abscissa goes from normal tissue through an admixture of infarct foci in the normal tissue (labeled infarct border) and continues in the epicardial layer overlying the infarct center. (B) The progression is from normal tissue through the border zone into the homogenous necrotic core. (From ref. 21 with permission)

pyrophosphate in the border zone of the infarct in infusion studies, but also with bolus injections it behaves more like thallium-201 (Figure 1.13). Figure 1.14 shows a good correlation between CT and autopsy measures of infarct size.<sup>21</sup> However, delayed enhancement was only seen consistently 24 hours after coronary artery obstruction, and was not seen during transient occlusion for up to 10 minutes.<sup>25</sup>

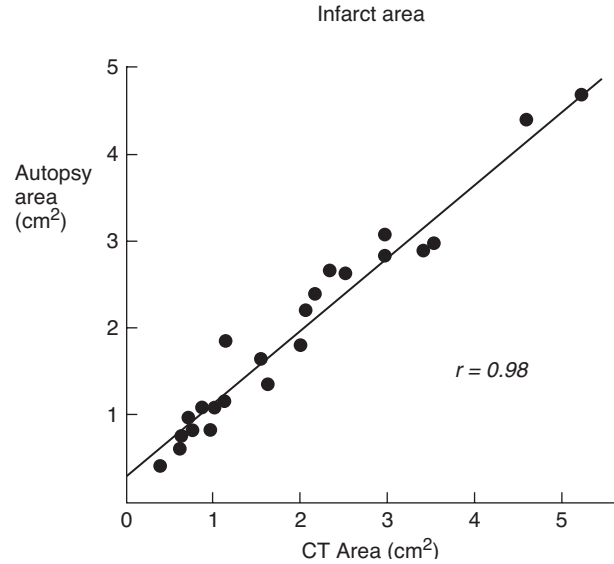


**Figure 1.14** Comparison of computerized transmission tomography (CTT) and autopsy in the measurement of infarct area in individual tomographic slices from intact living dogs. The excellent correlation is attributable, in part, to the use of only transmural infarctions, which simplifies the task of boundary placement for area calculations by both CTT and autopsy. Infarct volume can be determined by summing the areas in contiguous 1-cm slices. (From ref. 21 with permission)

Similar appearances occurred in patients with AMI, as seen in Figure 1.15, and in chronic infarction and remodeling (Figure 1.16). Their observations were confirmed in more recent studies with Multidetector CT (MDCT) scanners in animals and patients.<sup>26–27</sup> Kramer et al. used single slice non-gated CT to study a series of 19 patients with CT elevation and myocardial infarction within 1 month of the event and confirmed these findings.<sup>28</sup> More recently Koyama, obtaining similar results with Multidetector CT, also reported similar findings in patients.<sup>29</sup>

## II CT SCANNERS PROPOSED FOR IMAGING THE HEART

The requirements for imaging the heart with CT are listed in Table 1.3. Several methods were developed to overcome limited temporal resolution. Ritman and CT collaborators built a CT research machine using multiple X-ray tubes and image intensifiers for dynamic spatial reconstruction of the heart.<sup>30–31</sup> This pioneered many aspects of cardiac CT, but this scanner was never duplicated. A more practical

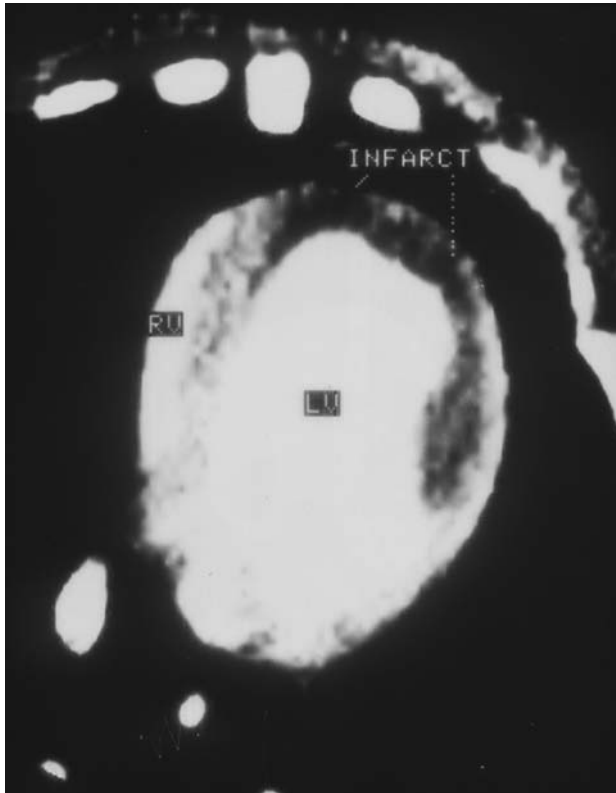


**Figure 1.15** A 1 cm thick CT scan following a 20 ml bolus of intravenous contrast in a patient with a 36 hour antero septal myocardial infarct. Note the negative perfusion defect in the infarcted territory and normal enhanced myocardium elsewhere during the first passage of contrast. RV = right ventricle and LV = left ventricle.

scanner was proposed by Douglas Boyd in 1978, employing a scanning electron beam.<sup>32-33</sup> This device is now very familiar and, known as EBCT, remains the only CT scanner designed specifically for millisecond cardiac CT scanning. The first machine was built and installed at UCSF. This scanner was introduced commercially in 1984. Since then new models appeared in 1988 and 2003 offering dual 1.5 mm slices and multilevel scanning at exposure speeds of 33 m sec. The capability of EBCT is summarized in Table 1.4. Approximately 300 EBCT scanners were installed world wide, representing only 1.5% of the entire CT market. ECG-gating was unnecessary with EBCT although CT acquisition could be triggered to the ECG.

The concept of improving mechanical scanners by ECG-gating methods found poor clinical utility with single slice machines. One solution for shortening exposure times and breath holding requirements was proposed by Redington.<sup>34</sup> This involved adding multiple X-ray tubes (3 or more) with opposed detectors arrays. This idea has

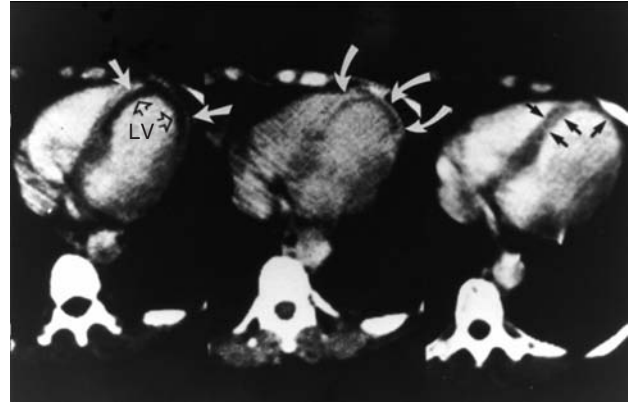


**Figure 1.16** Contrast enhanced CT scan left panel in a patient 72 hours after acute myocardial infarction. The image on the left demonstrates hypo-enhancement (straight white arrows) in the antero-septal regions of ischemic injury after contrast infusion (white arrows). A second scan middle panel, at the same level, shows delayed enhancement of this zone at 10 mins. (curved arrows) after contrast has washed out of normal myocardium and the cardiac chambers. The right panel is the same patient 3 months later demonstrating left ventricular (LV) remodeling with thinning of the infarcted walls (black arrows). Left ventricular aneurysm formation and some compensatory hypertrophy of the free LV wall is present.

also been introduced recently in dual source multidetector CT (MDCT).

The concept of continuous spiral scanning began in the 1980s using slip-ring technology to transfer power continuously during rotation. With the advent of smaller, high frequency power units, this type of scanner became practical.<sup>35</sup> In 2000, Willi Kalender, using a slip-ring scan, demonstrated the value of spiral CT.<sup>36</sup> Within a few years 8 then 16 and 64 slice MDCT machines became available, allowing

**Table 1.3** Requirements for computed tomographic scanning of the heart

- 1) Rapid scan time, 33 to 100 ms or less with repeatability.
- 2) Multislice capability, eight or more simultaneously.
- 3) Repeat multislice study at 1 second during passage of contrast bolus.
- 4) Scan registration using computed radiography for slice localization.
- 5) Three-dimensional transformations into sagittal, coronal and oblique images.
- 6) Software for quantitative analysis.
- 7) Contrast medium enhancement (contrast medium with 40% iodine concentration)

**Table 1.4** EBCT capability

- 1) Rapid scan time (50 ms).
- 2) Multislice capability (8 or more simultaneously).
- 3) Repeat multislice at 1 second (or faster) during passage of contrast bolus.
- 4) Three-dimensional transformation into sagittal, coronal, and oblique images.
- 5) Quantitative analysis software.
- 6) Subtraction.
- 7) Functional imaging analysis and display.

many benefits, including isotropic resolution, which is important for 3D image processing. It preserves image quality during multiplanar reconstruction from the original CT acquisition plane. The combination of 16 slice MDCT and ECG-gating methods made cardiac imaging feasible for the first time with mechanical CT scanners. It was now possible to acquire a volume of contiguous 0.5 mm thick slices in 10 seconds, with a significant reduction in contrast medium requirements as well as breath holdings time. The coronary arteries could be imaged even though scan speed remains at 300 m sec for a partial scan reconstruction; however with ECG-gating it was lowered by a factor of 2 to 150 m sec or 75 m sec by integrating CT data acquired during 2 or 4 consecutive heart beats.

EBCT enabled accurate quantitation of coronary calcification, and could display the coronary arteries with contrast enhancement as well as the pulmonary veins. An example is seen in Figure 1.17. This image was obtained in the early 1980s. EBCT demonstrated the value of post

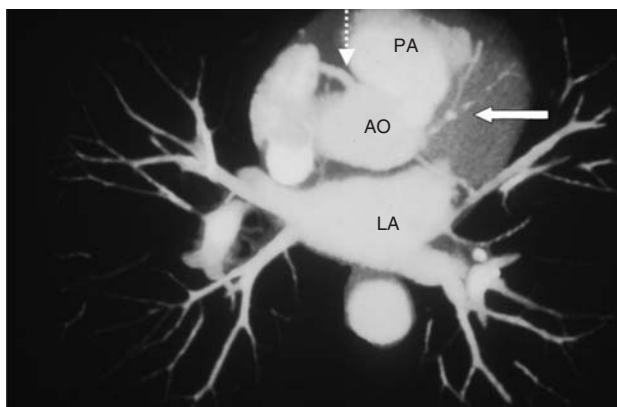


**Figure 1.17** Post processed subtracted EBCT axial image demonstrating the right (dotted arrow) and left coronary arteries. There is calcification and beading of the left anterior descending artery (solid arrow). PA = pulmonary artery, AO – aorta, LA = Left atrium with 4 draining pulmonary veins.

processing techniques long before they became routine clinical tools and also the potential for CT angiography (CTA).<sup>37–38</sup> It seemed likely then, that once higher CT temporal resolution became widely available, measurements of all these structures and CTA would become routine in everyday clinical care. However, few were convinced at that time.

## 12 LEFT VENTRICULAR REMODELING

Myocardial infarction may result in compensatory hypertrophy, wall thinning and /or decreased myocardial thickening. This was well demonstrated by CT with conventional ECG-gating CT and with EBCT. Figure 1.18 illustrates a series of contrast-enhanced images during one cardiac cycle. The EBCT scanner table was designed to angulate and can therefore directly image the short axis plane without loss of CT image resolution in the acquired transaxial plane by 3D reconstruction. Endocardial and epicardial borders can be defined and segmented, hence ventricular indices could therefore be obtained at each scan level from the cardiac apex to base. The CT results compared favorably with established methods, as shown Figure 1.19. CT can therefore be used to evaluate patients in longitudinal studies. Reiter validated the accuracy of EBCT for left and right stroke volume measurements against implanted calibrated electrodes in dogs and also by thermodilution an excellent correlation was found, as seen in Figure 1.20. Simultaneous measures of right and left ventricular volumes were obtained from the same CT data acquisitions.<sup>39</sup> Caputo and Roig et al. in separate studies demonstrated the feasibility of performing exercise stress CT.<sup>40–42</sup> Lanzer et al.<sup>43</sup> demonstrated the feasibility of performing CT with pharmacological interventions.<sup>44–45</sup> The effect of pacing can also be assessed by CT, as shown in Figure 1.21. Further physiological animal studies were performed with EBCT to explore the pressure and volume effects of pericardial effusion on cardiac function involving LV failure.<sup>44–45</sup>

## 13 CT MEASUREMENT OF BLOOD FLOW

Single slice CT and later EBCT was also used to explore the potential of CT to measure blood flow in vessels, cardiac chambers and tissues. Jashke et al. used indicator dilution theory to study CT in a phantom.<sup>46</sup> Later blood flow was measured by CT in non-moving organs, notably the spleen,

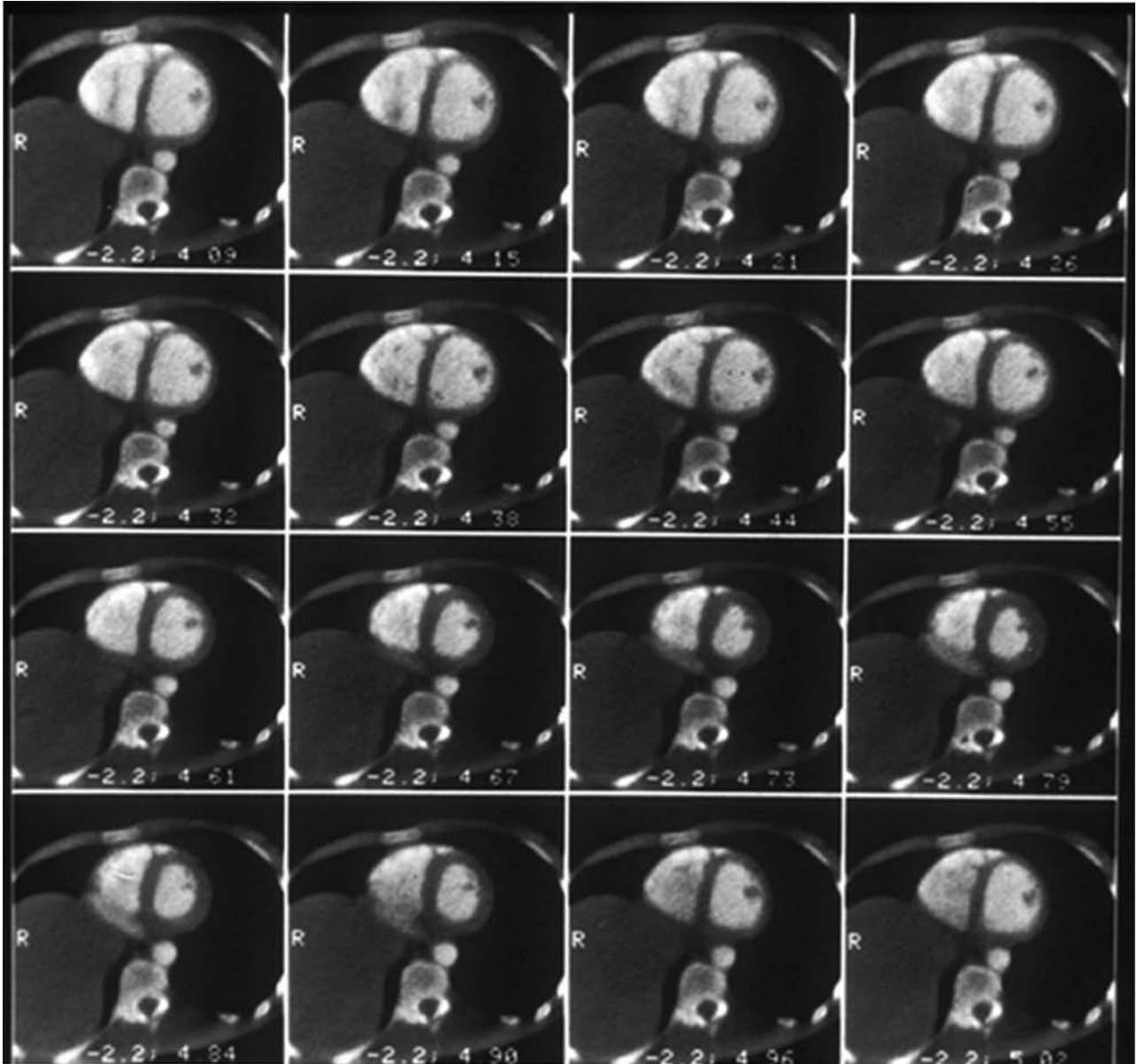


**Figure 1.18** EBCT images acquired at 100 m sec interval in the short axis plane demonstrating the typical appearances of the right and left ventricular cavities through the cardiac cycle.

liver and kidney.<sup>47</sup> In the myocardium a gamma variant fit can be obtained from the first passage of a short intravenous contrast medium bolus, as shown in Figure 1.22. This was used by Gould et al. to study myocardial blood flow at rest and during maximum vasodilatation, and obtained a good correlation on a regional basis with microspheres, as can be seen for one dog in Figure 1.23, and for a series of 9 dogs in Figure 1.24. Other early feasibility studies showed similar results; more recently ECG-gated MDCT also appears to validate this earlier work with similar studies.<sup>48-50</sup>

Ringertz showed reciprocal changes in blood flow in one carotid artery during contralateral occlusion and stenosis.<sup>51</sup>

The results were validated by electromagnetic flow probes on each carotid artery. One approach is illustrated in Figure 1.25 where the peak arrival time at multiple levels along the vessel can be measured by CT time-density curves and from this, the velocity is calculated. Measurements of the vessel area obtained from the axial CT images provide an area and velocity which is a useful measure of blood flow. The area under the time-density curve reflects cardiac output, and this too was validated against thermodilution, initially with a single slice scanner and later EBCT.<sup>52-53</sup> The linear regression line for CT density in Hounsfield numbers against iodine concentration is excellent over a wide range. Coronary artery by-pass

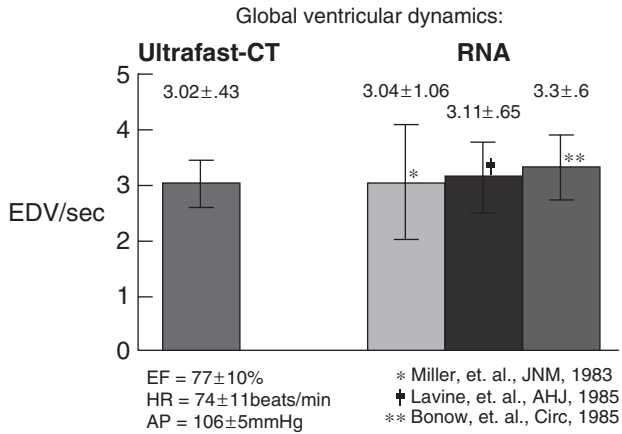


**Figure 1.19** Global ventricular dynamics by EBCT in a patient series, compared with established values by radionuclide methods. A good correlation can be seen.

graft patency with CT was first reported in a patient series by Brudage et al. and W. Stanford.<sup>54-55</sup> Measurements of graft flow were explored by Rumberger et al.<sup>56-57</sup>

## 14 CONGENITAL HEART DISEASE AND CT

The utility of CT for identifying intracardiac shunts was measured by Garrett et al. in a dog model, in which a

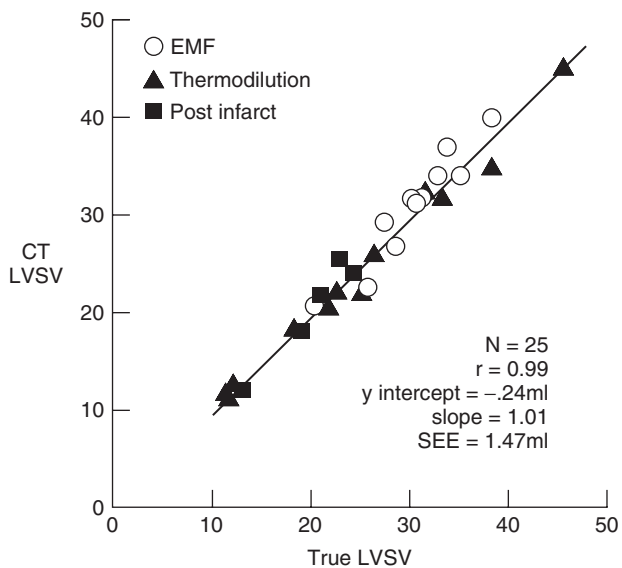


**Figure 1.20** CT-derived left ventricular stroke volume (LVSV) compared with true LVSV determined by electromagnetic flow probe (EMF) or thermodilution cardiac output. Precision of measurements of right and left ventricular volume by cine computed tomography. (From ref. 39 with permission)

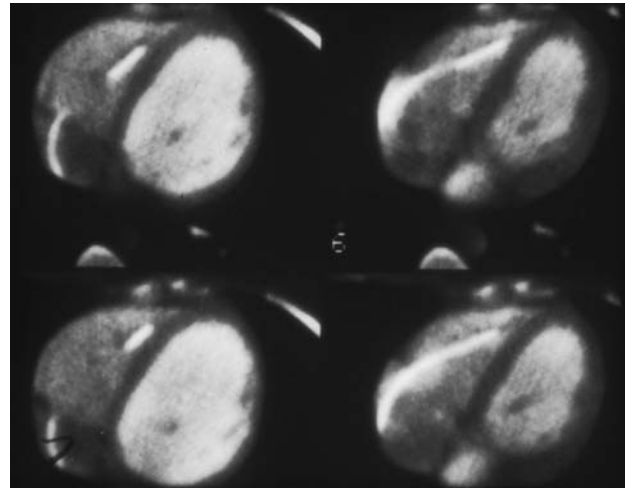


**Figure 1.21** Contrast enhanced 8 mm thick EBCT scans at the same level during one cardiac cycle demonstrated the position of a pacing catheter in the right heart. Motion degradation due to pacemaker artifacts is not a significant problem.

variable shunt was created between the left atrium and pulmonary artery. CT measurements of shunt flow, using the recirculation time/density curves (similar to nuclear medicine studies) derived from an ROI over the atrium, showed excellent correlation with measurements of oxygen saturation curves.<sup>58</sup>

A large patient series with congenital heart has also been studied with EBCT by Eldridge et al.<sup>59</sup>

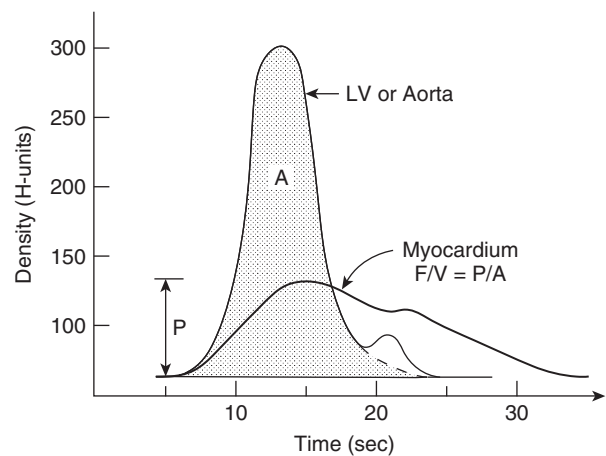


**Figure 1.22** Myocardial perfusion curve generated over a myocardial region of interest. Curve analysis provides peak height. Blood flow (F/V) in any myocardial region can be calculated as the ratio of the peak of the time density curve in that area (P) to the area under the aorta or left ventricle time density curve (A), which is representative of cardiac output. HU = Hounsfield units.

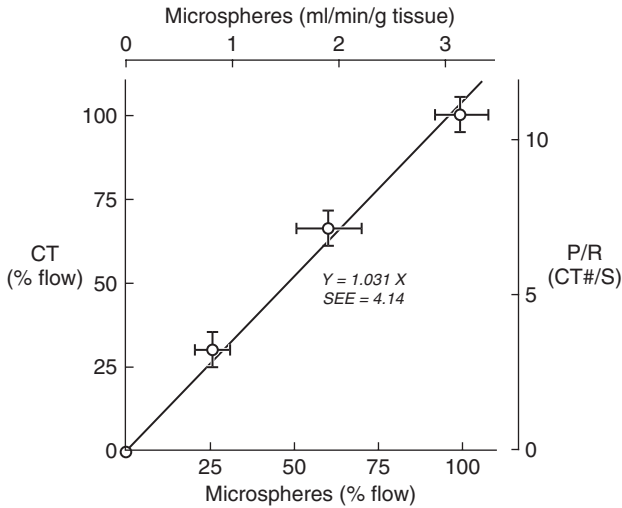


**Figure 1.23** Comparison of EBCT and radiolabeled microsphere measurements of global myocardial flow in a mongrel dog. The dotted line is the line of unity.

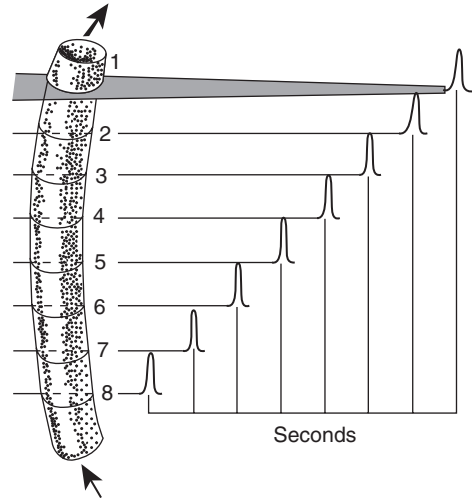


**Figure 1.25** Illustration of the CT time density curves generated at eight contiguous levels from a multilevel EBCT flow sequence. The diagram represents a vessel-like carotid artery. The peak arrival time is given for each flow curve; hence, the velocity profile can be measured in cm per sec. Blood flow can be estimated from the velocity if the vessel area is known. This is readily calculated from the many cross-sectional CT images.

## 15 PULMONARY HYPERTENSION

Pulmonary embolism was also evaluated by CT in acute and chronic patients in the early part of the 1980s.<sup>60-62</sup>

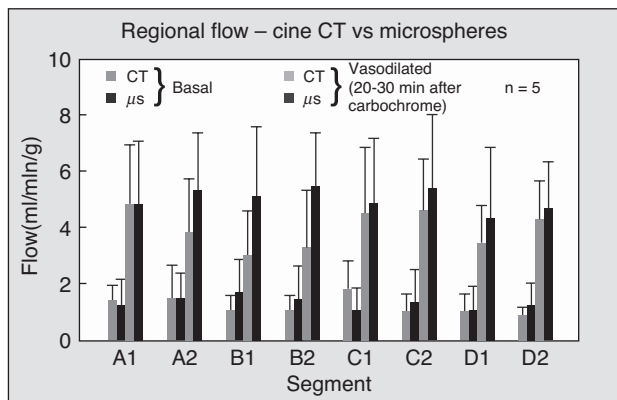


**Figure 1.24** Comparison of EBCT measurements of regional myocardial perfusion with microspheres in a series of dogs. Four areas of interest were identified at two LV levels on CT images during sequential scans triggered at end diastole to minimize motion. Chromonar was administered to provide data for each 8 regions at rest and during maximal vasodilatation. The microspheres were injected simultaneously and the results graphed as illustrated in pairs for resting and stress states by region. The error bars illustrate the excellent correlation achieved. Measurement of regional myocardial blood flow in dogs by ultrafast CT. (From ref. 48 with permission).

## 16 SUMMARY

Many individuals have contributed to the development of CT for cardiac applications. The early studies described here suggest that CT still has a great deal to offer patients with heart disease. Feasibility studies are important, but now there is good evidence that MDCT, which is widely available, will have the critical mass of proponents to pursue it on a larger scale. Quantitation of cardiac function by CT can be considered in two major categories. The first is by motion versus time, in which endsystolic and diastolic images provide linear, area and /or volume measurements of arteries, cardiac chambers and myocardial walls over time intervals.

The second method is by obtaining CT images during a fixed phase of the cardiac cycle, usually diastole on every heart beat or every other, and measuring the flow of contrast (density) versus time, using indicator dilution principles.

CT has only been available for the past 30 years. Many factors are involved in determining which diagnostic study is preferred for a given patient with heart disease. These include proven efficacy, robustness, reliability and accuracy, additionally the comfort and confidence of the referring physician, as well as patients' is important. Availability and cost are also relevant issues, as well as competing studies, which are far more established and accepted than newer techniques.

This historical review of feasibility and validation studies should provide a broad base and encouragement for those more recently involved in cardiac CT. The early studies were designed to evaluate the potential of CT with the expectation that it would one day become the success for the heart that it has been for other organ systems. To this end the literature referenced can be considered in four main categories, ranging progressively from: (1) mathematical simulations, (2) Phantom experiments, (3) animal studies, and (4) patient pilot studies and clinical trials.

The chapters which follow expand greatly on the current and future clinical applications of CT for cardiovascular diagnosis.

## REFERENCES

- Rosenbusch G, Odkerk M, Amman E. *Radiology in Medical Diagnostics – Evolution of X-ray application 1895–1995*. Blackwell Science, Berlin, 1990.
- Takashi S. *Rotational Radiography*. Society for the Promotion of Science, Tokyo, Japan, 1957.
- Hounsfield GN, Computed Medical Imaging. Nobel lecture, December 8, 1979. *Computed medical imaging*. *Med Phys*. 1980; 7(4): 283–90.
- Adams DF, Hessel SJ, Judy PF, et al. Computed Tomography of the Normal and Infarcted myocardium. *Am J Roentgenol* 1976; 126(4): 786–91.
- Wittenberg J, Powell WJ, Jr., Dinsmore RF, et al. Computerized tomography of ischemic myocardium: Quantitation of extent and severity of edema in an in vitro canine model. *Invest. Radiol*. 1977; 12: 215–23.
- Gray WR., Jr, Parkey RW, Buja IM., et al. Computed tomography: In vitro evaluation of myocardial infarction. *Radiol*. 1977; 122: 511–13.
- Powell WJ, Jr., Wittenberg J, Maturi RA., et al. Detection of edema associated with myocardial ischemia by computerized tomography in isolated, arrested canine hearts. *Circulation* 1977; 55(1): 99–108.
- Dodge HT, Sandler H, Baxley WA, Hawley RR. Usefulness and limitations of radiographic methods for determining left ventricular volume. *Am J Cardiol*. 1966; 18(1): 10–24.
- Holliday D, Resnich R. Archimedes' Principle. In: *Physics* (Wiley, New York, 1966); 430.
- Lipton MJ, Hayashi TT, Boyd DF, Carlsson E. Measurement of left ventricular cast volume by computerized tomography. *Radiol*. 1978; 127(2): 419–23.
- Lipton MJ, Hayashi TT, Davis PL, Carlsson E. The effects of orientation on volume measurements of human left ventricular casts. *Invest Radiol* 1980; 15(6): 469–74.
- Skjoldebrand CG, Ovenfors CO, Mavroudis C, Lipton MJ. Assessment of ventricular wall thickness in vivo by computed transmission tomography. *Circulation* 1980; 61(5): 960–65.
- Skjoldebrand CG, Lipton MJ, Mavroudis C, Hayashi TT. Determination of left ventricular mass by computed tomography. *Am J Cardiol* 1982; 49(1): 63–70.
- Berninger WH, Redington RW, Doherty P, Lipton MJ, Carlsson E. Gated cardiac scanning: canine studies. *J Comput Assist Tomogr*. 1979; 3(2): 155–63.
- Godwin JD, Herfkens RJ, Skioldebrand CG, et al. Detection of intraventricular thrombi by computed tomography. *Radiol*. 1981; 138(3): 717–21.
- Lackner K, Thurn P. Computed tomography of the heart: ECG-gated and continuous scans. *Radiol*. 1981; 140(2): 413–20.
- Masuda Y, Yoshida H, Morooka N, et al. ECG synchronized computed tomography in clinical evaluation of total and regional cardiac motion: comparison of postmyocardial infarction to normal hearts by rapid sequential imaging. *Am Heart J*. 1982; 103(2): 230–8.
- Mattrey RF, Slutsky RA, Long SA, Higgins CB. In vivo assessment of left ventricular wall and chamber dynamics during transient myocardial ischemia using prospectively ECG-gated computerized transmission tomography. *Circulation* 1983; 67(6): 1245–51.
- Berninger WH, Redington RW, Leue W, et al. Technical aspects and clinical applications of CT/X, a dynamic CT scanner. *J Comput Asst Tomogr* 1981; 5: 206–15.
- Carlsson E, Lipton MJ, Berninger WH, Doherty P, Redington RW. Selective left coronary myocardiography by computed tomography in living dogs. *Invest Radiol* 1977; 12(6): 559–62.
- Doherty PW, Lipton MJ, Berninger WH, et al. The detection and quantitation of myocardial infarction in vivo using transmission computed tomography. *Circulation* 1981; 63(3): 597–606.
- Newell JD, Higgins CB, Abraham JL, et al. Computerized tomographic appearance of evolving myocardial infarctions. *Invest. Radiol*. 1980; 15: 207–14.
- Lipton MJ, Higgins CB. Evaluation of ischemic heart disease by computerized transmission tomography. *Radiologic Clinics of NA* 1980; 18(3): 557–76.
- Siemers PT, Higgins CB, Schmidt W, Ashburn W, Hagan P. Detection, quantitation and contrast enhancement of myocardial infarction utilizing computerized axial tomography: comparison with histochemical staining and <sup>99m</sup>Tc-pyrophosphate imaging. *Invest Radiol*. 1978; 13(2): 103–9.
- Ringertz HG, Palmer RG, Lipton MJ, Carlsson E. CT attenuation ratio of myocardium and blood pool in the normal and infarcted canine heart. *Acta Radiologica [Diagn]* 1983; 24(1): 11–16.
- Gerber BL, Belge B, Legros GJ, et al. Characterization of acute and chronic myocardial infarcts by multidetector computed tomography: comparison with contrast-enhanced magnetic resonance. *Circulation* 2006; 113(6): 823–33.
- Lardo AC, Cordeiro MA, Silva C, et al. Contrast-enhanced multidetector computed tomography viability imaging after myocardial infarction: characterization of myocyte death, microvascular obstruction, and chronic scar. *Circulation* 2006; 113(3): 394–404.
- Kramer PH, Goldstein JA, Herkens RJ, Lipton MJ, Brundage BH. Imaging of acute myocardial infarction in man with contrast-enhanced computed transmission tomography. *Am Heart J*. 1984; 108(6): 1514–23.
- Koyama Y, Matsuoka H, Mochizuki T, et al. Assessment of reperfused acute myocardial infarction with two-phase contrast-enhanced helical CT: prediction of left ventricular function and wall thickness. *Radiology* 2005; 235(3): 804–11.

30. Ritman EL. The DSR – a unique x-ray computed tomographic scanner for exploring the power of the dynamic spatial reconstruction. *Am J Card Imaging* 1994; 8(2): 161–7.
31. Ritman EL. Cardiac computed tomography imaging: a history and some future possibilities. *Cardiol Clin.* 2003; 21(4): 491–513.
32. Boyd DP. A proposed dynamic cardiac 3-D densitometer for early detection of and evaluation of heart disease. *IEEE Trans Nucl Sci.* 1979; 26: 2724.
33. Boyd DP, Couch JL, Napel SA, Peschmann KR, Rand RE. Ultrafast cine CT: Where have we been? What lies ahead? *Am J Card Imaging*, 1987; 1: 175.
34. Redington RW, Berninger WH, Lipton MJ, et al. Cardiac computed tomography. *SPIE: Recent and future developments in medical imaging II.* 1979; 206: 67–72.
35. Boyd DP. *Instrumentation and Principles of CT, Chapter II. Cardiac PET and PET/CT Imaging.* Di Carli M, Lipton MJ, eds, published by Springer (in press).
36. Kalender WA, Seissler W, Klotz E, Vock P. Spiral volumetric CT with single-breath-hold technique, continuous transport, and continuous scanner rotation. *Radiology* 1990; 176(1): 181–3.
37. Hubener KH, Lipton MJ. Digital radiography (scanning projection): Possibilities and perspective. In: *Radiology Today*, 2nd ed, FH Heuck and MW Donner, eds. Heidelberg (Springer-Verlag, 1983) 298–306.
38. Lipton MJ, Boyd DP. Contrast media in dynamic computed tomography of the heart and great vessels. *Proceedings of the CT International Workshop, Berlin, Exerpta Medica* 1981; 204–13.
39. Reiter SJ, Rumberger JA, Feiring AJ, Stanford W, Marcus ML. Precision of measurements of right and left ventricular volume by cine computed tomography. *Circulation* 1986; 74(4): 890–900.
40. Roig E, Chomka EV, Castaner A, et al. Exercise ultrafast computed tomography for the detection of coronary artery disease. *J Am Coll Cardiol.* 1989; 13(5): 1073–81.
41. Caputo, Gould R, Dery R., et al. Ultrafast CT evaluation of exercise induced ischemia: a feasibility study. *Dynamic Cardiovascular Imaging* 1989; 2(2): 110–19.
42. Lipton MJ, Rumberger JA. Exercise Ultrafast Computed Tomography: Preliminary findings on its role in diagnosis of Coronary Artery Disease. *Editorial. JACC.* 1989; 13(5): 1082–84.
43. Lanzer P, Garrett J, Lipton MJ, et al. Quantitation of regional myocardial function by cine computed tomography: Pharmacologic changes in wall thickness. *J Am Coll Cardiol* 1986; 8(3): 682–92.
44. Smiseth OA, Refsum H, Junemann M, et al. Ventricular diastolic pressure-volume shifts during acute ischemic left ventricular failure in dogs. *JACC* 1984; 3(4): 956–77.
45. Smiseth OA, Frais MA, Junemann M, et al. Left and right ventricular diastolic function during acute pericardial tamponade. *Clinical Physiology* 1991; 11(1): 61–71.
46. Jaschke W, Gould RG, Assimakopoulos PA, Lipton MJ. Flow measurements with a high speed computed tomography scanner. *Med Physics* 1987; 14(2): 238–43.
47. Jaschke W, Cogan MG, Sievers R, Gould R, Lipton MJ. Measurement of renal blood flow by cine computed tomography. *Kidney Intl* 1987; 31(4): 1038–42.
48. Gould RG, Lipton MJ, McNamara MT, et al. Measurement of regional myocardial blood flow in dogs by ultrafast CT. *Invest Radiol* 1988; 23(5): 348–53.
49. Rumberger JA, Feiring AJ, Lipton MJ, et al. Use of ultrafast CT to quantitate regional myocardial perfusion: a preliminary report. *JACC* 1987; 9(1): 59–69.
50. Koyama Y, Mochizuki T, Higaki J. Computed tomography assessment of myocardial perfusion, viability, and function. *J Magn Reson Imaging* 2004; 19(6): 800–15.
51. Ringertz H, Jaschke W, Sievers RE, Lipton MJ. Relative carotid blood flow measurements in dogs by high-speed CT. *Invest Radiol* 1987; 22(12): 960–64.
52. Herfkens RJ, Axel L, Lipton MJ, et al. Measurement of cardiac output by computed transmission tomography. *Invest Radiol* 1982; 17(6): 550–3.
53. Garrett JS, Lanzer P, Jaschke W, et al. Measurement of cardiac output by cine computed tomography. *Am J Cardiol* 1985; 56(10): 657–61.
54. Brundage BH, Lipton MJ, Herfkens RJ, et al. Detection of patent coronary bypass grafts by computed tomography. A preliminary report. *Circulation* 1980; 61(4): 826–31.
55. Stanford W, Brundage BH, MacMillan R, et al. Sensitivity and specificity of assessing coronary bypass graft patency with ultrafast computed tomography: results of a multicenter study. *JACC* 1988; 12(1): 1–7.
56. Rumberger JA and Lipton MJ. *Ultrafast cardiac CT scanning.* *Cardiology Clinics*, Wolfe C. ed. (W. B. Saunders Company, Philadelphia, PA 1989), 7(3): 713–34.
57. Rumberger JA, Feiring AJ, Hiratzka, et al. Quantification of coronary artery bypass flow reserve in dogs using cine-computed tomography. *Circ Res.* 1987; 61(5 Pt 2): II, 117–23.
58. Garrett JS, Jaschke W, Aherne T, et al. Quantitation of intracardiac shunts by cine-CT. *JCAT* 1988; 12(1): 82–7.
59. Eldridge WJ, Diethelm NE, Lipton MJ. Ultrafast computed tomography in the diagnosis of congenital heart disease. In: *Pediatric Cardiovascular Imaging.* Tonkin ILD, Ed. (WB Saunders Company: Philadelphia, 1992) 177–201.
60. Di Carlo LA, Schiller NB, Herfkens RJ, Brundage BH, Lipton MJ. Noninvasive detection of proximal pulmonary artery thrombosis by two-dimensional echocardiography and computerized tomography. *Am Heart J* 1982; 104(4) Part 1: 879–81.
61. Kareiakis DJ, Herfkens RJ, Brundage BH, Gamsu G, Lipton MJ. Computerized tomography in chronic thromboembolic pulmonary hypertension. *Am Heart J* 1983; 106(6): 1432–36.
62. Himmelman RB, Abbott JA, Lipton MJ, Schiller NB. Cine computed tomography compared with echocardiography in the evaluation of cardiac function in emphysema. *Am Jnl of Cardiac Imaging* 1988; 2(4): 283–91.

# 2

## Physics of and Approaches to Cardiovascular Computed Tomography

---

Marc Kachelrieß

### I INTRODUCTION

Cardiac computed tomography (CT) challenges the problem of imaging moving objects without showing motion artifacts. The aim is to provide high fidelity images that allow to perform coronary CT angiography, coronary calcification measurements, soft plaque detection and dynamic CT studies of the heart.

In general, CT requires at least  $180^\circ$  plus fan angle of projection data to perform image reconstruction. This implies that the intrinsic temporal resolution of a standard CT scan is in the order of  $t_{rot}/2$  or worse, where  $t_{rot}$  is the time needed for a full rotation of the scanner and lies in the order of 0.33 s to 0.5 s, today. With modern cone-beam CT scanners it is possible to achieve  $t_{rot}/2 = 165$  ms which is not sufficient to perfectly image the anatomical details of the moving human heart. Standard spiral CT image reconstruction further makes use of all the data contributing to a given voxel and therefore exhibits a temporal resolution of about  $t_{rot}/p$  where  $p$  is the spiral pitch value defined by the ratio of the table increment per rotation and the total collimation (number of slices times slice thickness). The value  $1/p$  quantifies the number of rotations that contribute to a single point in the object. Typical pitch values lie in the range from 0.1 to 1.5.

Special reconstruction algorithms have been designed to allow reducing the data to a single  $180^\circ$  segment to always come close to  $t_{rot}/2$ . If the object is moving in

a periodic fashion it is further possible to use dedicated cardiac reconstruction algorithms that divide the required  $180^\circ$  into one, two or more smaller segments and collect these smaller data segments from adjacent motion periods (e.g. heart cycles) and that ensure that the same motion phase always enters the image. Thereby, the temporal resolution can be improved proportionally to the number of segments used and 4D phase-correlated imaging of the heart is achieved. The alignment of these allowed data intervals (be it one or several segments) to a desired motion phase generates images where the object's motion is frozen in the desired motion state. These basic concepts of phase-correlated CT imaging were first proposed and evaluated in Kachelrieß and Kalender<sup>1</sup> and since then they are widely used in clinical CT.<sup>2-12</sup>

To further improve the temporal resolution, new scanner concepts that simultaneously utilize two x-ray sources and two detector arrays were introduced in 2005. These dual source CT (DSCT) scanners require only a  $90^\circ$  rotation to acquire sufficient data and hence exhibit a temporal resolution in the order of  $t_{rot}/4$  or less. Thereby, 83 ms temporal resolution are routinely achieved which is sufficient to image patients with high heart rates and with arrhythmia throughout all motion cycles.

This chapter gives an introduction into the basics of cardiac CT as it is in use today. It focuses on physics, technology and image reconstruction. Dose issues and cardiac CT applications are addressed elsewhere in this book.

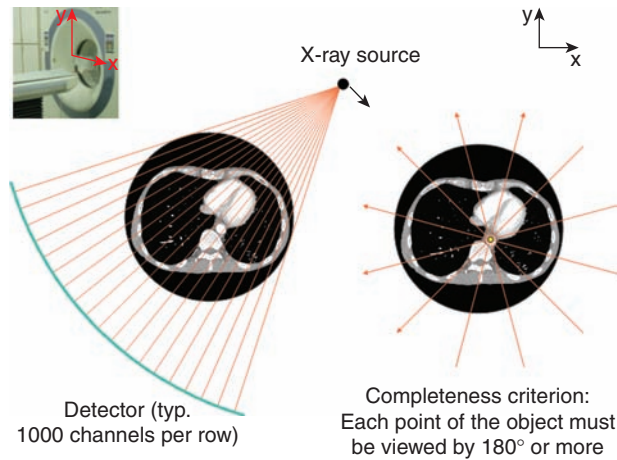


**Figure 2.1** Clinical CT is the measurement of x-ray photon attenuation along straight lines. The in-plane scan geometry is the fan-beam geometry with one point-like source and many detector elements. During a rotation of the gantry many line integrals are measured – enough to perform image reconstruction.

around the patient. On the opposing side of the x-ray tube a cylindrical detector consisting of about  $10^3$  channels per slice is mounted (Figure 2.1). The plane of rotation is the x-y-plane.

The number of slices that are simultaneously acquired is denoted as  $M$  (Figure 2.2). In the longitudinal direction (perpendicular to the plane of rotation), the size of the detectors determines the thickness  $S$  of the slices that are acquired. During a full rotation approximately of  $10^3$  read-outs of the detector are performed. Altogether about  $10^6$  intensity measurements are taken per slice and rotation. The negative logarithm  $p(L)$  of each intensity measurement  $I$  corresponds to the line integral along line  $L$  of the object’s linear attenuation coefficient distribution  $\mu(x, y, z)$ :

$$p(L) = -\ln \frac{I(L)}{I_0} = \int_L dL \mu(x, y, z).$$

$I_0$  is the primary x-ray intensity and is needed for proper normalization.

The CT image  $f(x, y, z)$  is a close approximation to the true distribution  $\mu(x, y, z)$ . The process of computing the CT image from the set of measured projection values  $p(L)$  is called image reconstruction and is one of the key components of a CT scanner. For circle scans that perform measurements at a fixed z-position, image reconstruction is rather simple. It consists of a convolution of the projection data

## 2 CT BASICS

Clinical CT is the measurement of an object’s x-ray absorption along straight lines. As long as each object point is probed by x-rays under an angular interval of  $180^\circ$  image reconstruction of that point is possible. Therefore, clinical CT scanners have an x-ray focal spot that rotates continuously

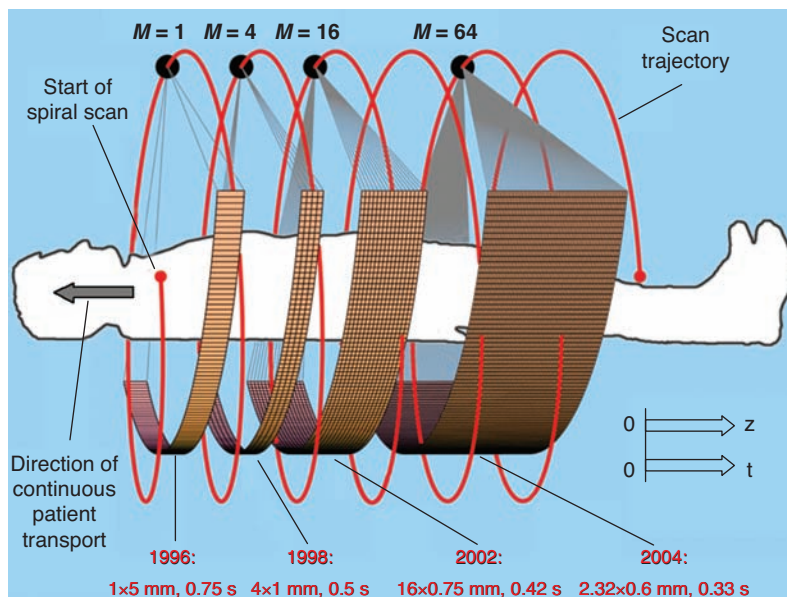


**Figure 2.2** Spiral CT principle. Four scanner generations are shown: single-slice, 4-slice, 16-slice and 64-slice spiral CT scanners.

with the reconstruction kernel followed by a backprojection into image domain:

$$f(x, y) = \int_0^\pi d\vartheta p(\vartheta, \xi) * k(\xi) \Big|_{\xi = x \cos \vartheta + y \sin \vartheta}$$

where  $\vartheta$  is the angle and  $\xi$  is the distance of the measured ray  $L$  that is defined as  $x \cos \vartheta + y \sin \vartheta = \xi$ . The algorithm is called the filtered backprojection (FBP) and is implemented in all clinical CT scanners. Several reconstruction kernels  $k(\xi)$  are available to allow modifying image sharpness (spatial resolution) and image noise characteristics.

The reconstructed image  $f(x, y, z)$  is expressed in CT values. They are defined as a linear function of the attenuation values. The linear relation is based on the demand that air (zero attenuation) has a CT value of  $-1000$  HU (Hounsfield units) and water (attenuation  $\mu_{\text{water}}$ ) has a value of  $0$  HU. Thus, the CT value is given as a function of  $\mu$  as follows:

$$CT = \frac{\mu - \mu_{\text{water}}}{\mu_{\text{water}}} 1000 \text{ HU.}$$

The CT values are often called the Hounsfield values. They have been introduced by Hounsfield to replace the handling with the rather inconvenient  $\mu$  values by an integer-valued quantity. Since the CT value is directly related to the attenuation values, which are proportional to the density of the material, we can interpret the CT value of a pixel or voxel as being the (approximate) density of the object at the respective location. It should be noted here that CT, in contrast to other imaging modalities such as magnetic resonance imaging or ultrasound imaging, is highly quantitative regarding the accuracy of the reconstructed values. The reconstructed attenuation map can therefore serve for quantitative diagnosis such as the quantification of coronary calcifications.

### 3 SPIRAL CT

In the late 1980s, just when continuously rotating scanners became available, a new scan mode was introduced by Willi A. Kalender.<sup>9,13,14</sup> In spiral CT data acquisition is performed continuously while the patient moves at constant speed through the gantry. Viewed from the patient the scan trajectory is a spiral. Although not obvious spiral scans turned out to yield better image quality than conventional scans. This, however, requires the addition of z-interpolation as an additional image reconstruction step.<sup>9</sup>

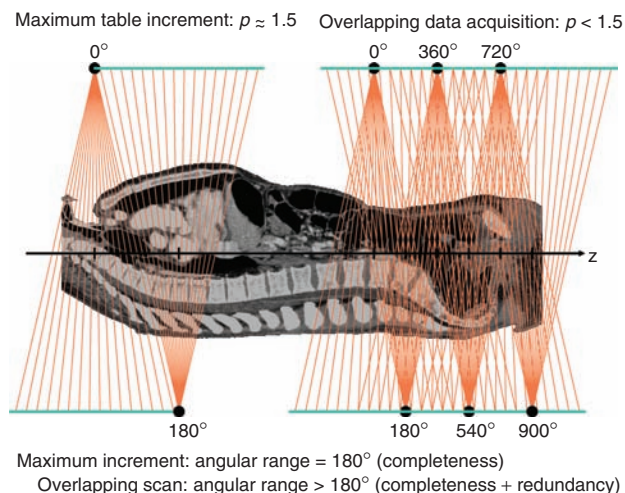


**Figure 2.3** The pitch value's upper limit is determined by the completeness criterion (c.f. Figure 2.1). Smaller pitch values mean that redundant data are acquired. Cardiac CT makes use of the data redundancy to select only interesting data intervals, i.e. those that are in the desired phase of cardiac motion.

A new scan parameter has been introduced in spiral CT: the table increment  $d$  is the distance the table travels during one rotation of the gantry. In conventional CT (circle scans) this value has typically been equal to the collimated thickness (adjacent but non-overlapping images). In spiral CT we can choose  $d$  smaller or greater than  $M \cdot S$ . One uses the so-called pitch value to relativize the definition of the table increment<sup>15</sup>:

$$p = \frac{d}{W_{\text{ax}}}$$

$W_{\text{tot}}$  is the total collimation and usually equal to the product of the number of slices  $\times$  nominal slice thickness, i.e.  $W_{\text{tot}} = M \cdot S$ . Small pitch values yield overlapping data and the redundancy can be used to decrease image noise (more quanta contribute to one z-position), to reduce artifacts or, in case of cardiac CT, to improve temporal resolution (Figure 2.3). Large pitch values increase the scan speed and complete anatomical ranges can be covered very fast. Typical values lie between 0.1 and 1.5 and spatial resolution is not a function of the pitch value. However, for some scanners pitch values up to 2 are allowed and the longitudinal spatial resolution (z-resolution) decreases whenever the pitch exceeds the value 1.5.

The inverse pitch  $1/p$  measures how many rotations contribute to each z-position. For example with  $p = 1$  we find

that a given z-position is covered by exactly one rotation and for  $p = 0.5$  two rotations contribute to the z-position, i.e. a  $720^\circ$  angular interval.

## 4 CARDIAC CT

The aim of cardiac CT is to provide images of the heart that are free of motion artifacts and that correspond to a specified motion phase. Only then can applications such as coronary CT angiography or coronary calcification quantification be carried out reliably and guarantee reproducible results.

To achieve this goal one must be able to synchronize data acquisition and/or image reconstruction with the cardiac motion and one must achieve a fairly high temporal resolution. Synchronization is typically done using the patient ECG signal that is recorded simultaneously with CT data acquisition (Figure 2.4). Alternative approaches that derive the motion signal directly from the patient raw data or from a set of reconstructed images are in use, too.<sup>16,17</sup>

Typical heart rates lie in the range from 40 bpm to 120 bpm and correspond to a duration of the heart cycle between 0.5 s and 1.5 s. To avoid blurring due to heart motion it is desired to have no more than 10% of the motion cycle show up in the reconstructed images and the temporal resolution should be in the order of 50 ms to 150 ms, depending on the heart rate. Since this cannot always be achieved, high heart rates (above 70 bpm) are frequently avoided by using premedication with beta blockers. CT imaging requires projection data from at least  $180^\circ$  plus fan angle. Using this minimal data interval guarantees

a temporal resolution of slightly above  $t_{rot}/2$  where  $t_{rot}$  is the time needed for one scanner rotation. An example that shows the differences between a standard reconstruction that uses all available data and a phase-correlated reconstruction that only shows the minimal data required is given in Figure 2.5.

### 4.1 Prospective triggering

One way to obtain phase-correlated CT images of the heart is to use the ECG to trigger the scan (x-ray and data acquisition on). This prospective technique is typically used in combination with circle scans. The scanner is continuously rotating, the patient table is at rest and the x-rays and data acquisition are switched on whenever the ECG signal is about to arrive at the desired motion phase. X-rays and data acquisition are switched off after  $180^\circ$  plus fan angle of data have been acquired. After one acquisition the table is advanced by a certain amount (that typically corresponds to the total collimation) and the procedure is repeated until the complete heart is covered. The temporal resolution lies in the order of  $t_{rot}/2$  and image reconstruction is a simple partial scan reconstruction (filtered backprojection of  $180^\circ$  plus fan angle).

Since prospective gating is nothing but a sequential CT scan (step-and-shoot scan, multiple circle scan) triggered by an external signal it does not benefit from the higher image quality that can be achieved with spiral CT. For example data inconsistencies due to patient motion between different table positions may show up in the

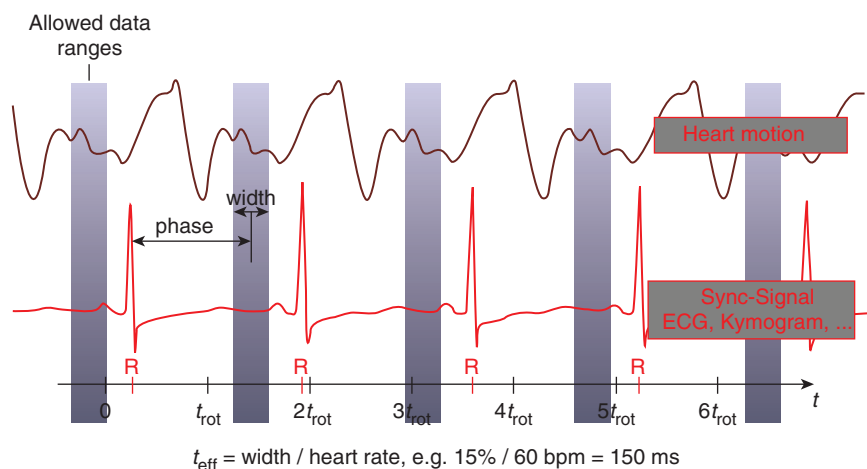


**Figure 2.4** In cardiac CT only data corresponding to a certain motion phase shall contribute to the images. In prospective gating techniques this phase is fixed, for retrospective gating one can vary the phase from reconstruction to reconstruction. The width of the data intervals determines the temporal resolution.

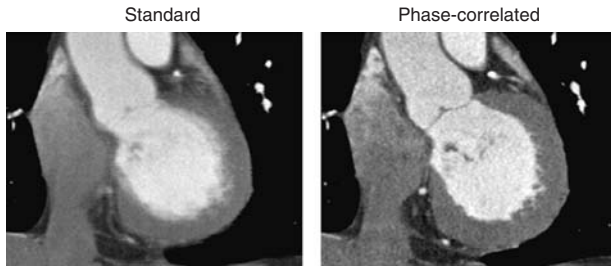


**Figure 2.5** Example images of the heart using a standard reconstruction (left) and a phase-correlated reconstruction (right). Due to the low temporal resolution the standard image is a superposition of all cardiac phases and hence all structures are significantly blurred. This is not the case for the phase-correlated image.  $C = 150$  HU,  $W = 700$  HU.

reconstructed images and volumetric displays of the data may not be of state-of-the-art quality.

## 4.2 Retrospective gating

One of the most prominent special CT applications today is retrospectively gated CT of the heart. It combines the advantages of spiral CT with phase-correlated imaging and thereby guarantees highest image quality, isotropic spatial resolution, fast scanning and high temporal resolution. Cardiac spiral CT started with the introduction of dedicated

phase-correlated reconstruction algorithms for single-slice spiral CT in 1997<sup>1</sup> and since then they have been extended to multi-slice and cone-beam CT and are widely used in clinical routine.<sup>2-12</sup>

The underlying principle of phase-correlated spiral CT is to acquire highly overlapping spiral data using a small pitch value. In this case the acquired data are highly redundant and a given voxel or z-position is covered by far more than the  $180^\circ$  actually needed. Dedicated image reconstruction algorithms make use of this data redundancy by selecting a small  $180^\circ$  interval from the large and redundant data range (Figure 2.6).

Freely selecting such a data interval within the cardiac motion cycle implies that the time  $t_{rot}/p$  the scanner covers a given z-position (or a given voxel) is longer than the duration  $1/f_H$  of one heart cycle: Whenever the spiral pitch, the patient heart rate and the scanner rotation time fulfill the requirement

$$P < f_H \cdot t_{rot}$$

it is possible to retrospectively select a  $180^\circ$  interval at any desired cardiac motion phase. Only then can one reconstruct the complete heart as a function of time.

As an example, consider a patient with a heart rate of 60 bpm and assume the scanner rotation is 0.33 s. Choosing a pitch value of 0.2 or 0.3 would be adequate in this case, a pitch value of 0.4 would be too high to allow for

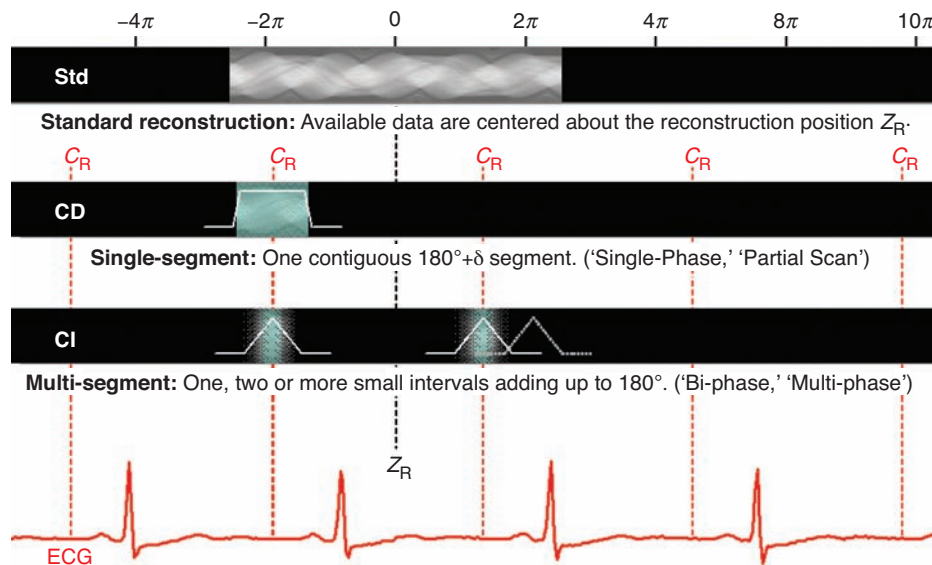


**Figure 2.6** Principle of retrospectively gated cardiac CT. Standard reconstruction utilizes all available data, i.e.  $1/p$  full rotations. Cardiac reconstruction combines one or more data segments to yield a complete  $180^\circ$  data range with maximum temporal resolution.

phase correlation. Note that lower heart rates require lower pitch values and thus imply slower scanning.

With this so-called partial scan, single-segment or single-phase approach one achieves a temporal resolution of  $t_{rot}/2$ . In case of a 0.33 s rotation these are 165 ms. However, one can further increase the temporal resolution by splitting up the required  $180^\circ$  into two or more data segments that are collected from adjacent heart beats (Figure 2.6). These so-called multi-segment or multi-phase approaches have the advantage of increasing the temporal resolution by up to a factor two or three, respectively. Of course, the scan speed must be decreased to allow for two or three heart beats during the coverage of a given z-position and the relation  $P < f_H \cdot t_{rot}$  must be replaced by  $P < f_H \cdot t_{rot}/2$  or  $P < f_H \cdot t_{rot}/3$ , respectively. In practice, the algorithms are adaptive and automatically choose the appropriate data segments as a function of the scan pitch, the rotation time and the patient heart rate<sup>1</sup>: low heart rates typically imply single-segment reconstruction, high heart rates are handled with multi-segment approaches, in case of varying heart frequency the algorithms may adaptively switch between single- and multi-segment mode.

However, the technique to collect data from multiple heart cycles suffers from the fact that a lower pitch value is required and that their benefit is dependent on the heart rate. In a case where the heart rate is in resonance with the scanner rotation, e.g. when the patient has 60 bpm and the scanner rotates with 0.5 s, the multi-phase approaches exhibit the same temporal resolution as the single-phase approaches because after one heart beat the scanner ‘sees’ exactly the same view angles as have been acquired already during the first heart cycle. Therefore, the temporal resolution exhibits a rather complex behavior (top curve in Figure 2.7) and in case of resonances the multi-segment algorithms exhibit the same low temporal resolution as the single-segment reconstruction.<sup>5-18</sup>

### 4.3 Dual-source CT

From Figure 2.1 we have learned that a  $180^\circ$  data interval is required to perform image reconstruction. Typically, this requirement limits the temporal resolution to 50% of the scanner rotation time. However, when more than one x-ray tube and more than one detector, i.e. more than one spiral thread, are built into the same gantry one can acquire the  $180^\circ$  data range with less than  $180^\circ$  rotation (Figure 2.8). With multi-source CT scanners the achievable temporal resolution increases proportionally with the

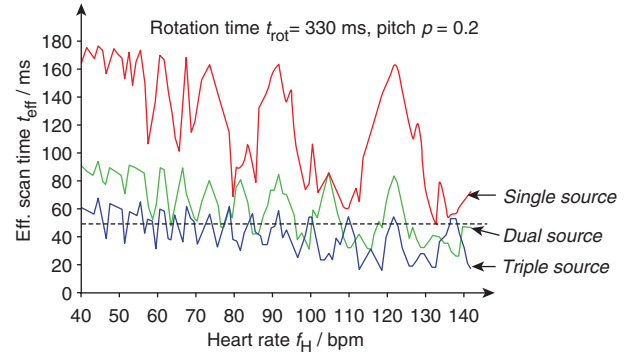


**Figure 2.7** Temporal resolution in phase-correlated cardiac spiral CT as a function of heart rate for scanners with one, two and three source-detector systems. The temporal resolution of multi-phase approaches is always equal to or better than the temporal resolution of a single phase or partial scan algorithm.<sup>5,18</sup>

number of sources used. For multi-segment phase-correlated image reconstruction the heart rate dependency turns out to be far smaller with multi-source CT scanners than with single source CT scanners (Figure 2.7, bottom two curves).<sup>18</sup>

Regarding the literature the first multi-source CT systems that were realized attempted achieving fully four-dimensional imaging by completely sampling large object regions in the spatial and temporal domain with high spatial

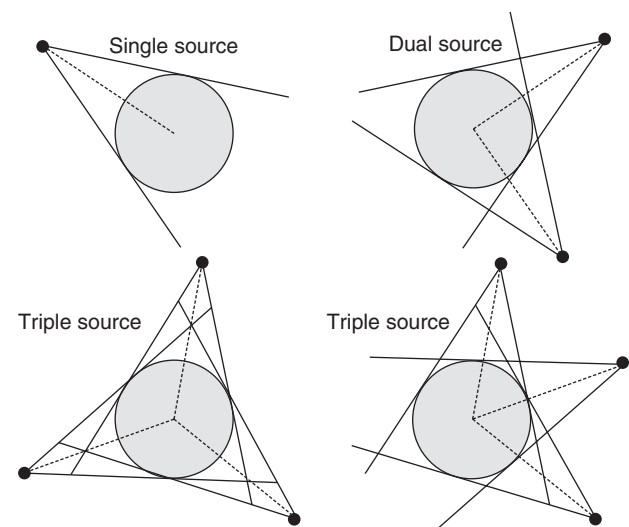


**Figure 2.8** CT systems with two or three x-ray sources require only a  $90^\circ$  or  $60^\circ$  acquisition interval to obtain complete data. Hence, their temporal resolution is increased by a factor of two and three, respectively, compared to single source CT scanners.

and temporal resolution.<sup>19-21</sup> Cost and image quality issues did not allow to commercialize this system. Liu et al.<sup>22</sup> also proposed a multi-threaded CT scanner to improve temporal resolution but no system was realized. Neither of these systems considered phase-correlated image reconstruction, no design optimizations regarding temporal resolution were carried out and no reconstructions of clinical cardiac CT data were provided.

Recently, the first clinical dual source dual detector CT system became available. It uses two threads, a z- and an  $\alpha$ -flying focal spot (see Flohr et al.<sup>23</sup> and Kachelrieß<sup>24</sup> for details regarding the flying focal spot), and it reads out 32 detector rows per thread (Somatom Definition, Siemens Medical Solutions, Forchheim, Germany).<sup>25</sup> Each projection thus consists of 2·32 slices (Figure 2.9).

The Definition scanner rotates at 0.33 s and thereby achieves a temporal resolution of 83 ms for single-phase (partial scan) cardiac image reconstruction. This is high enough to obtain superb artifact-free images for a wide range of heart rates, even in cases of arrhythmia. For example Figure 2.10 shows a clear delineation of the coronary arteries even into the most distal segments. Even more, reconstructions can be performed at any cardiac phase with nearly equal image quality (Figure 2.11). Higher temporal resolution can be achieved with DSCT using multi-segment reconstruction techniques, just in the single-source case and may be of use for functional assessment of the heart. In any case, the DSCT experience gathered so far meets the expectations and proves a significant benefit over single-source CT systems.<sup>26,27</sup>

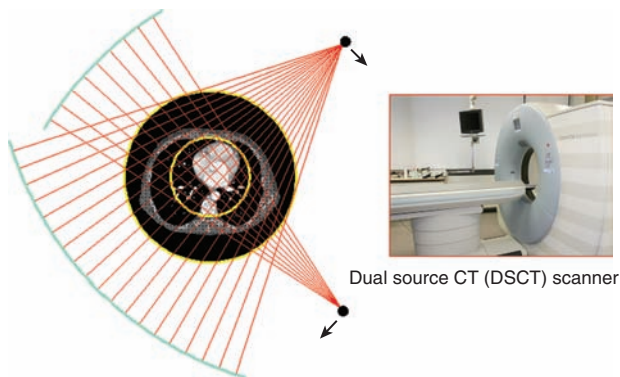


**Figure 2.9** The DSCT scanner Somatom Definition (Siemens Medical Solutions, Forchheim, Germany) comprises two tube detector systems mounted at an angle of 90° and thereby requires only a quarter rotation to acquire a complete CT data set. With 0.33 s required for a full rotation its temporal resolution is 0.33 s/4 = 83 ms.

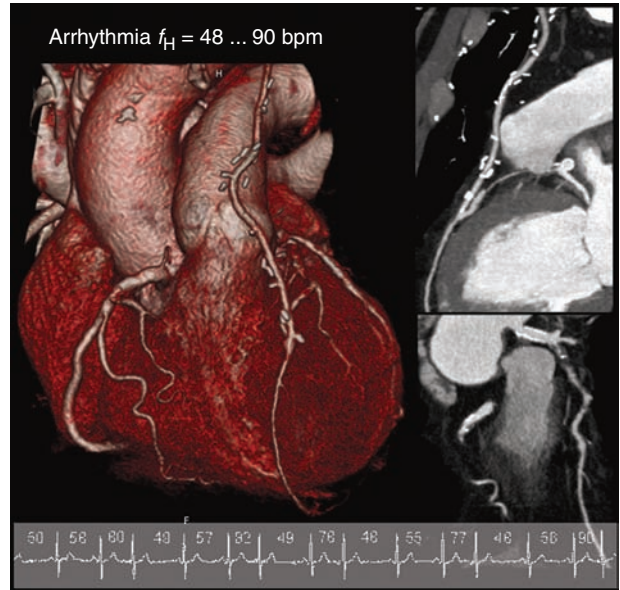


**Figure 2.10** Heart rate independent cardiac imaging with dual source CT: arrhythmic patient, heart rate from 48 bpm to 90 bpm, 83 ms temporal resolution, 0.33 s rotation, 13 s for 137 mm. Data courtesy of University of Erlangen, Germany.

#### 4.4 Kymogram-correlated cardiac CT

Typically, phase-correlated cardiac CT imaging uses the patient ECG signal for synchronization and for correlation. However, the ECG is an electric signal and does not exactly map to the mechanical motion of the heart. Signals that

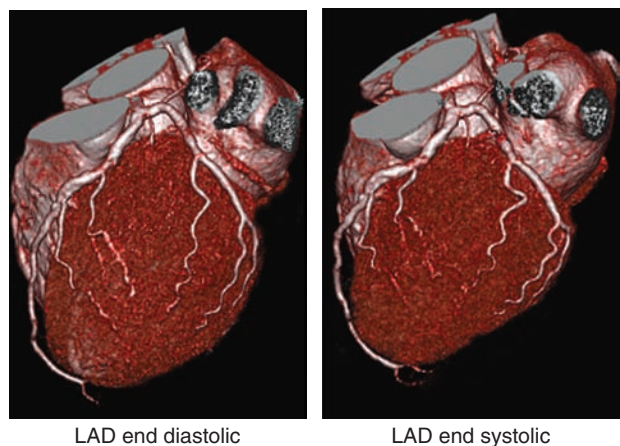


**Figure 2.11** Heart rate independent cardiac imaging with dual source CT throughout all cardiac phases: patient heart rate from 79 bpm to 86 bpm, 83 ms temporal resolution, 0.33 s rotation, 6 s for 120 mm. Data courtesy of University of Erlangen, Germany.

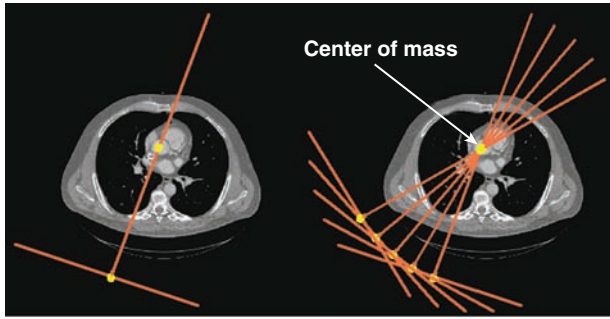


**Figure 2.12** Kymogram principle. A few projections suffice to triangulate the center of mass of the heart. Since this COM moves as a function of time one can use the resulting kymogram as a synchronization signal for cardiac imaging.

directly reflect the cardiac motion, which is the source of motion artifacts, may be promising alternatives for synchronization. A raw data-based signal that fulfills this criterion is the so-called kymogram function.<sup>16</sup> It is based on the center of mass theorem that allows to deduce the object center of mass (COM) from the projection center of mass. All that is required are a number of adjacent CT projections. From these projections one can obtain the object center of mass by

simple triangulation (Figure 2.12). Due to the heart motion the so derived object COM moves as a function of time and this motion signal, the kymogram, can be used to synchronize image reconstruction.

A recent study shows that kymogram-based image reconstruction and ECG-based image reconstruction are of comparable quality with ECG-based imaging being slightly superior.<sup>28</sup> Even though this is true on average, in about 5% of the cases the kymogram provides diagnostic images while the ECG does not (Figure 2.13). Therefore one may regard the kymogram as a backup solution for those cases or for cases where the ECG is not available at all or where it is deficient.

## 4.5 Optimal reconstruction phase

Since the heart's contractile motion is a non-uniform quasi-periodic motion, not all phase intervals in the cardiac cycle are equally well suited with respect to the phase-correlated reconstruction algorithm. The systolic phase corresponds to the contraction of the heart and the myocardium shows a high velocity. After relaxation the heart is almost at rest which corresponds to the diastolic phase. The diastolic phase represents the optimal cardiac reconstruction phase

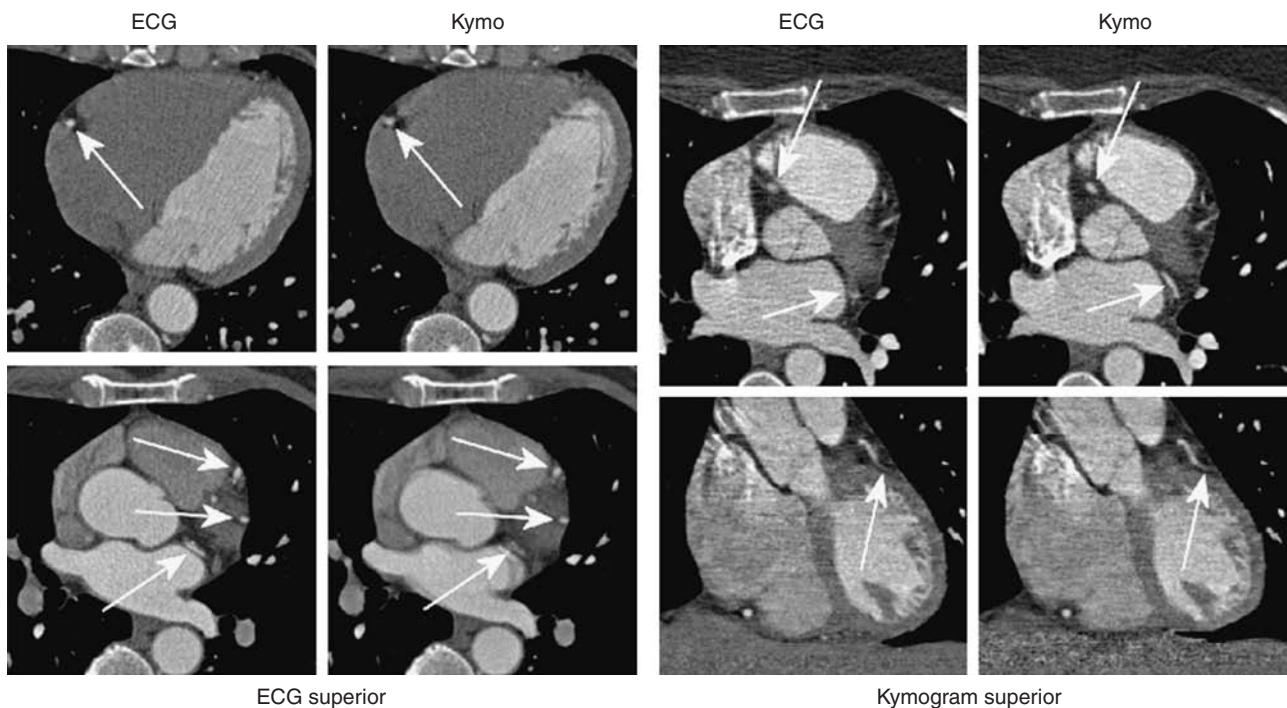


**Figure 2.13** In most cases both synchronization approaches are comparable. For some patients the ECG performs better than the kymogram (left), for other patients the kymogram is superior (right). All four reconstructions show the optimal reconstruction phase (found by manual selection).  $C = 150$  HU,  $W = 700$  HU.

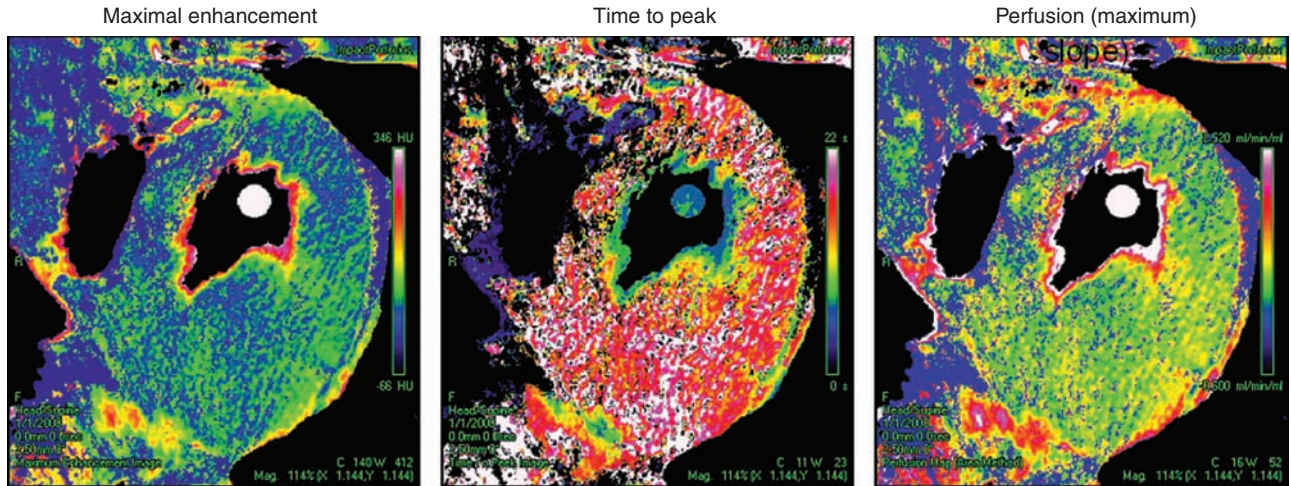


**Figure 2.14** Assessment of cardiac function requires 5D imaging (spatial domain + cardiac motion phase + contrast bolus).<sup>31,32</sup>

for most cases,<sup>29</sup> since the temporal window for the data acquisition covers the period of rest. With increasing heart rate, the systolic phase more frequently provides optimal image quality. However, a general prediction of the optimal reconstruction phase showing a minimum of motion is not possible. On the one hand, the possibility of an optimal reconstruction in either the systolic or the diastolic phase (both is possible depending on the patient), prohibits this prediction. On the other hand, a slight patient-dependent variation of the typical ECG phases makes the prediction uncertain. Hence, it is common practice to approach the optimal image quality adaptively by image reconstruction at different phase points. To overcome these problems fully, automatic algorithms, among them the said raw data-based kymogram approach, have been proposed providing the optimal reconstruction phase.<sup>17,30</sup> Hereby, cardiac images with an optimal image quality can be achieved with a single image reconstruction process.

## 5 SUMMARY AND OUTLOOK

Motion artifact-free phase-correlated CT images of the heart require fast rotating scanners in combination with dedicated image reconstruction algorithms that are able to synchronize the cardiac motion with the raw data. In most cases the ECG signal is used for synchronization but alternative approaches, such as the raw data-based kymogram signal or the image-based motion map, are available, too.

Single-segment reconstruction algorithms obtain a temporal resolution of roughly half of the scanner rotation time. Multi-segment approaches that collect data from adjacent heart cycles may obtain a significantly higher temporal resolution, given that the heart beat is not in resonance with the scanner rotation and given a rather low pitch value. Temporal resolution can be further increased by using dual-source CT scanners and the first clinical studies show that this DSCT technology appears to keep its promises or even outperform them.

Today, the fastest scanners rotate at 0.33 s and one routinely achieves a temporal resolution of far below 100 ms. In combination with isotropic sub-millimeter spatial resolution the resulting CT images of the heart are of highest diagnostic value.

In the future, scanners are likely to improve in temporal and in spatial resolution. Better detector technology, faster rotation times and multiple source-detector arrangements will be required. Increasing the number of simultaneously acquired slices — today 64 slices is standard — will allow to scan the complete heart with just one circle trajectory. This opens the door to phase-correlated dynamic scans of the heart<sup>31,32</sup> (Figure 2.14).

## REFERENCES

1. Kachelrieß M and Kalender WA. Electrocardiogram-correlated image reconstruction from subsecond spiral CT scans of the heart. *Med Phys* 1998; 25(12): 2417–31.

2. Flohr T, Stierstorfer K, Bruder H, and Kachelrieß M. A new cone-beam spiral CT reconstruction approach for 16 slice CT scanner with full dose utilization at arbitrary pitch. *Radiology* 2001; 221(P): 543.
3. Grass M, Manzke R, Nielsen T, et al. Helical cardiac cone-beam reconstruction using retrospective ECG gating. *Phys Med Biol* 2003; 48(18): 3069–84.
4. Flohr T, Ohnesorge B, Bruder H, et al. Image reconstruction and performance evaluating for ECG-gated spiral scanning with 16-slice CT system. *Med Phys* 2003; 30(10): 2650–62.
5. Kachelrieß M, Ulzheimer S, and Kalender WA. ECG-correlated image reconstruction from subsecond multi-slice spiral CT scans of the heart. *Med Phys* 2000; 27(8): 1881–1902.
6. Kachelrieß M, Ulzheimer S, and Kalender WA. ECG-correlated imaging of the heart with subsecond multi-slice spiral CT. *IEEE Trans Med Imaging (Special issue)* 2000; 19(9): 888–901.
7. Kachelrieß M, Fuchs T, Lapp R, et al. Image to volume weighting generalized ASSR for arbitrary pitch 3D and phase-correlated 4D spiral cone-beam CT reconstruction. In: *Proc. of the 6th Int. Meeting on Fully 3D Image Reconstruction* 2001: 179–82.
8. Kachelrieß M, Knaup M, and Kalender WA. Extended parallel backprojection for standard 3D and phase-correlated 4D axial and spiral cone-beam CT with arbitrary pitch and 100% dose usage. *Med Phys* 2004; 31(6): 1623–41.
9. Kalender WA. *Computed Tomography. Fundamentals, System Technology, Image Quality, Applications.* 2nd ed. Publicis Erlangen 2005.
10. Manzke R, Grass M, Nielsen T, Shechter G, and Hawkes D. Adaptive Temporal Resolution Optimization in Helical Cardiac Cone Beam CT Reconstruction. *Med Phys* 2003; 30(12): 3072–80.
11. Taguchi K and Anno H. High temporal resolution for multi-slice helical computed tomography. *Med Phys* 2000; 27(5): 861–72.
12. Achenbach S, et al. Noninvasive coronary angiography by retrospectively ECG-gated multislice spiral CT. *Circulation* 2000; 102(12): 2823–28.
13. Kalender WA, Seissler W, and Vock P. Single-breath-hold spiral volumetric CT by continuous patient translation and scanner rotation. *Radiology* 1989; 173(P): 414.
14. Kalender WA, Seissler W, Klotz E, and Vock P. Spiral volumetric CT with single-breath-hold technique, continuous transport, and continuous scanner rotation. *Radiology* 1990; 176(1): 181–3.
15. IEC. International Electrotechnical Commission, 60601-2-44: Medical electrical equipment – Part 2-44: Particular requirements for the safety of X-ray equipment for computed tomography, Geneva, Switzerland, 1999.
16. Kachelrieß M, Sennst D-A, Maxlmoser W, and Kalender WA. Kymogram detection and kymogram-correlated image reconstruction from subsecond spiral computed tomography scans of the heart. *Med Phys* 2002; 29(7): 1489–503.
17. Manzke R, Köhler T, Nielsen T, Hawkes DJ, and Grass M. Automatic phase determination for retrospectively gated cardiac CT. *Med Phys* 2004; 31(12): 3345–62.
18. Kachelrieß M, Knaup M, and Kalender WA. Multi-threaded cardiac CT. *Med Phys* 2006; 33(7): 2435–47.
19. Boyd DP. Transmission computed tomography. In: *Radiology of the skull and brain. Technical aspects of computed tomography.* Vol. 5. T. Newton and D. Potts, Editors. C.V. Mosby Company, St. Louis, 1981: 4357–71.
20. Robb R and Ritman EL. High speed synchronous volume computed tomography of the heart. *Radiology* 1979; 133: 655–61.
21. Robb R, Hoffmann E, Sinak LJ, Harris LD, and Ritman EL. High-speed three-dimensional x-ray computed tomography: The dynamic spatial reconstructor. *Proc. IEEE* 1983; 71: 308–19.
22. Liu Y, Liu H, and Wang G. Half-scan cone-beam CT fluoroscopy with multiple X-ray sources. *Med Phys* 2001; 28(7): 1466–71.
23. Flohr T, Stierstorfer K, Ulzheimer S, et al. Image reconstruction and image quality evaluation for a 64-slice CT scanner with z-flying focal spot. *Med Phys* 2005; 32(8): 2536–47.
24. Kachelrieß M, Knaup M, Penßel C, and Kalender WA. Flying focal spot (FFS) in cone-beam CT. *Trans Nuclear Science* 2006; 53(3): 1238–47.
25. Flohr T, et al. First performance of a dual-source CT (DSCT) system. *Eur Radiol* 2006; 16: 256–68.
26. Achenbach S, et al. Contrast-enhanced coronary artery visualization by dual-source computed tomography – Initial experience. *Eur J Radiol.* 2006; 57(3): 331–5.
27. Johnson TRC, et al. Dual-source CT cardiac imaging: initial experience. *Eur Radiol* 2006; 16: 1409–15.
28. Ertel D, Pflederer T, Kachelrieß M, et al. Validation of a rawdata-based synchronization signal (kymogram) for a phase-correlated cardiac image reconstruction. *IEEE Trans Med Imaging* 2006; submitted.
29. Achenbach S, Ropers D, Holle J, et al. In-plane coronary arterial motion velocity: Measurement with electron-beam CT. *Radiology* 2000; 216(2): 457–63.
30. Ertel D, Kachelrieß M, Pflederer T, et al. Raw data-based detection of the optimal reconstruction phase in ECG-gated cardiac image reconstruction. 9th International Conference on Medical Image Computing and Computer Assisted Intervention. In: *Proceedings MICCAI 2006.* Springer Berlin Heidelberg: 348–55.
31. Kachelrieß M. Phase-correlated dynamic CT. In: *Proc. of the IEEE International Symposium on Biomedical Imaging* 2004: 616–19.
32. Ulzheimer S, Muresan L, Kachelrieß M, et al. Considerations on the assessment of myocardial perfusion with multislice spiral CT (MSCT) scanners. *Radiology* 2001; 221(P): 458.

# 3

## Radiation Dose in Computed Tomography

---

Michael F. McNitt-Gray

The purpose of this chapter is to provide a discussion of radiation dose in X-ray computed tomography (CT), with specific application to CT of the cardiovascular system. Although CT represents a small percentage of radiological procedures performed, CT contributes a significant amount to the collective effective radiation dose from all radiological procedures.<sup>1</sup> Rapid advances in CT technology have increased both the utility and utilization of CT in many clinical diagnostic applications. Specifically, as tube rotation times climbed to the 0.5 second range and as the number of detector rows first reached 16 and then continued on to 64, the ability to perform CT scans for the coronary arteries has increased dramatically.<sup>2-4</sup> This has led to a significant increase in the number of patients being scanned for cardiovascular problems, both in a screening and diagnostic context.

This chapter will first describe some terms related to radiation dose and describe their methods of measurement. In the next section, the effects of some key CT technical factors on radiation dose will be described briefly. The following section will describe a few common uses of CT in cardiac imaging, providing estimates of radiation dose for each. Finally, a brief discussion will be provided for some additional advances in CT (e.g. Dual Source CT) as well as some radiation dose reduction technologies.

### I RADIATION DOSE BASICS

#### I.1 Radiation dose terms

##### I.1.1 Exposure

The term *exposure* is a term often used in the context of radiation dose discussions. It is defined as the ability of X-rays to ionize air and is measured in units of Roentgen or Coulomb/kg.<sup>5</sup> This term generally describes the concentration of radiation in air at a specific point. While it does describe how much ionization is created in air, it does not tell how much energy is absorbed by tissues, nor does it reflect the relative radiosensitivity of any particular tissue.

##### I.1.2 Radiation dose

The term *radiation dose* refers to the amount of energy absorbed per unit mass at a specific point.<sup>5</sup> This quantity is measured in Grays (SI unit, where 1 Gy = 1 Joule/kg) or rads (English unit, where 1 rad = 1 erg/gram), with the conversion between the two being 100 rads = 1 Gy. Radiation doses from CT in tissue are usually expressed in mGy (thousandths of a Gray) range. This quantity does describe how

much energy is absorbed from ionizing radiation in a small volume centered at a specific point. However, it generally does not specifically describe where that radiation dose is absorbed or reflect the relative radiosensitivity or risk of detriment to tissues being irradiated.

### 1.1.3 Effective dose

The term *effective dose* is not a physically measurable quantity, but is rather a construct designed to take into account not only where the radiation dose is being absorbed, but the relative radiosensitivity of the various tissues being irradiated.<sup>6,7</sup> It attempts to reflect the equivalent whole-body dose that results in a stochastic risk that is equivalent to the stochastic risk from a non-uniform, partial-body irradiation such as a CT scan. Effective dose is calculated by estimating the individual organ dose to a specific set of radiosensitive organs, and then taking a weighted average of organ doses, as described in Equation (1):

$$E = \sum_T w_T w_R D_{T,R} \quad (1)$$

where  $E$  is the effective dose,  $w_T$  is the tissue weighting factor,  $w_R$  is the radiation-weighting coefficient (1 for X-rays), and  $D_{T,R}$  is the average absorbed dose to tissue, where the subscript T represents each radiosensitive tissue, and the subscript R represents each type of radiation (in CT, only X-rays are present). The relative weighting factors are estimated for each radiosensitive organ in Publication 60 of the International Commission on Radiological Protection (ICRP).<sup>6</sup> It should be noted that these factors are under review and that significantly different weighing factors have recently been proposed by the BEIR VII (Biological Effects of Ionizing Radiation) report that is expected to be released in 2007. Effective dose is measured in Sieverts (Sv) or rems. The conversion between Sieverts and rem is  $100 \text{ rem} = 1 \text{ Sv}$ . Typical values of effective dose from CT scans range from  $< 1$  to  $10 \text{ mSv}$  ( $.001 \text{ Sv}$  to  $.01 \text{ Sv}$ ).

Although methods to calculate the effective dose have been established (ICRP Publications 60),<sup>6</sup> these methods depend heavily on the ability to estimate *the dose to the radiosensitive organs* from the CT procedure ( $D_{T,R}$ ). However, estimating the radiation dose to these organs is problematic and direct measurement is not possible. Several methods to estimate organ radiation dose, especially from CT are outlined in McNitt-Gray.<sup>8</sup>

### 1.1.4. CTDI

While the above definitions are general for any form of radiation, specific definitions for radiation dose from CT were developed because of its unique geometry and usage. While most conventional imaging methods (e.g. radiography) involve the use of a source at a single stationary position, in CT the source rotates around the patient. In addition, multiple exposures are acquired along the length of the patient to cover the desired anatomic region(s). This kind of usage resulted in a rotationally symmetric radiation dose distribution that extends along some length of the patient.

To help characterize this unique geometry and usage, methods were developed to calculate the radiation dose in a set of standardized phantoms, referred to as the Computed Tomography Dose Index (CTDI). In the original definition, developed by investigators in the FDA,<sup>9,10</sup> CTDI was defined as the average dose in the center slice of a series of several contiguous slices, when measured in one of two cylindrical phantoms. The large phantom is 32 cm in diameter and is referred to as the 'body' phantom. The smaller phantom is 16 cm in diameter and is referred to as the 'head' phantom. Both are made of polymethylmethacrylate (PMMA or an acrylic) and extend 15 cm in length. They each also have 5 holes drilled along the length of them to obtain a standard set of measurements; one in the center of the phantom and one each at ordinal positions 1 cm from the surface of the phantom at the 12:00, 3:00, 6:00 and 9:00 positions around the periphery of the phantom. Typically, measurements were made in the center position as well as in at least one of the four peripheral positions. Figure 3.1 shows a schematic of the CTDI measurement in a phantom, along with an example of a single axial scan radiation dose profile measured in the center position of the phantom and the dose distribution along the longitudinal direction that results from a series of contiguous axial scans, measured at the center position in the phantom.

These investigators<sup>9,10</sup> showed that in order to get the average dose in the center slice of a series of several contiguous slices, one need only estimate the area under the radiation profile along the z-direction (longitudinal axis) of a single axial tube rotation, integrate over the number of slices, and divide by the total nominal beam collimation. Therefore, a method was developed that allowed the use of a long, integrating pencil ionization chamber placed at the center of a single axial scan, to first measure the exposure along the length of the phantom (at a specific measurement position) and then use that measurement to calculate the CTDI value at a specific position (e.g. center or 12:00).

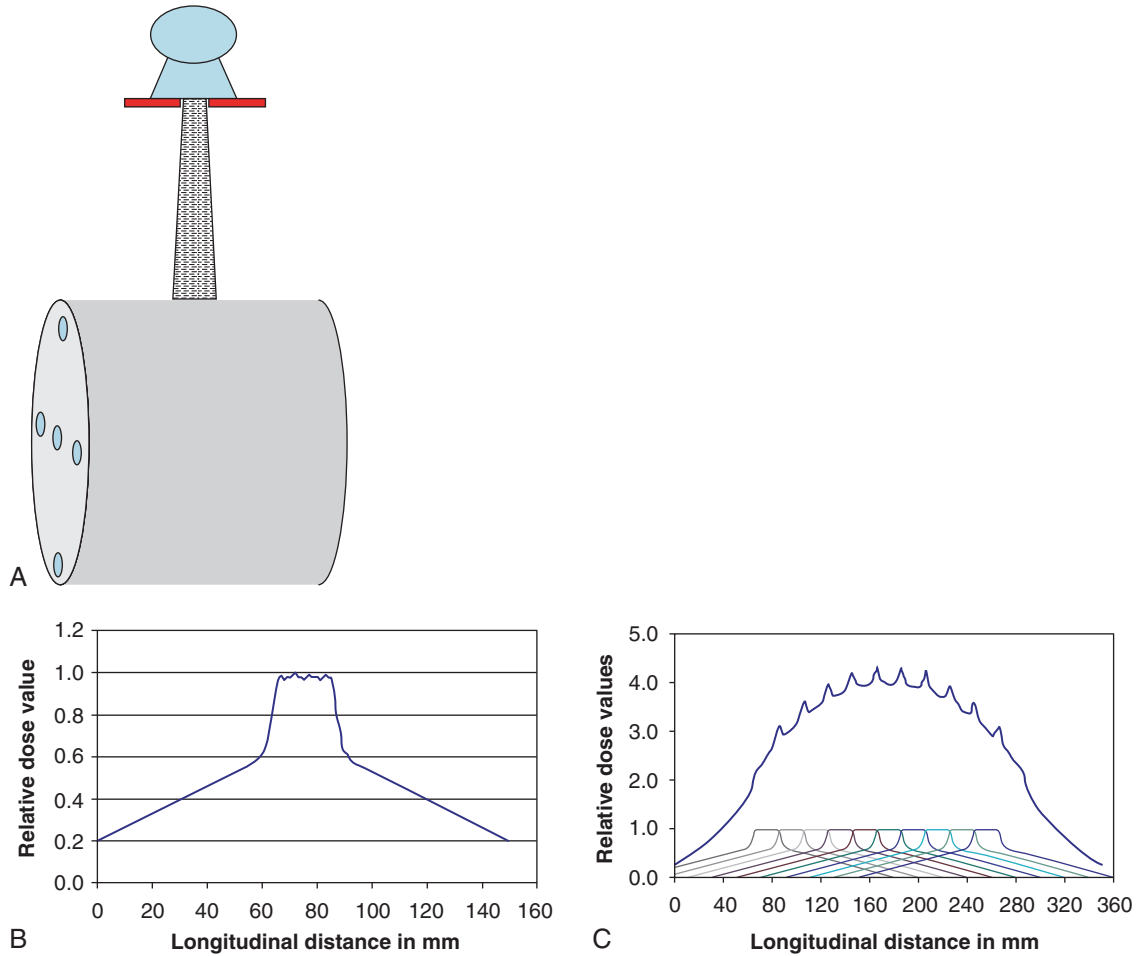


**Figure 3.1** (a) Diagram illustrating the CTDI measurement geometry where a single axial scan is performed around one of two phantoms; (b) the radiation profile measured along the longitudinal axis of the phantom at the center position resulting from a single axial scan; and (c) graph of the radiation profile measured along the longitudinal axis of the phantom at the center position resulting from a series of contiguous axial scans, where the graph shows both profiles from the individual scans and the total that results from the summation of all of these scans.

Originally, this was specified for 14 contiguous slices and is often referred to as  $CTDI_{FDA}$ . So that:

$$CTDI_{FDA} = \frac{1}{NT} \int_{-7T}^{7T} D(z) dz$$

where  $N$  = the number of simultaneous slices produced in a single rotation,  $T$  = width of each slice (so that the product of  $NT$  yields the nominal width of the x-ray beam), and  $D(z)$  is the measured radiation profile of a single axial tube rotation exposure using that nominal beam width  $NT$ .

Because the standard length of the measuring device (the pencil ionization chamber) is 100 mm, a slightly different CTDI index was developed.<sup>11</sup> In this metric, rather than specifying 14 slices at a specific beam width, it was recognized that the measurement was performed over 100 mm.

Therefore, the definition of  $CTDI_{100}$  was developed that was very similar to that of  $CTDI_{FDA}$ , but with fixed measurement limits that extend from  $-50$  mm to  $+50$  mm:

$$CTDI_{100} = \frac{1}{NT} \int_{-50mm}^{50mm} D(z) dz$$

This  $CTDI_{100}$  value is measured at the center and peripheral locations of each phantom.

Because the center and peripheral positions will result in different values (there is often a factor of two difference from center to periphery in a 32 cm phantom), a weighted average CTDI value was developed<sup>11</sup>:

$$CTDI_w = \left( \frac{1}{3} CTDI_{100,center} \right) + \left( \frac{2}{3} CTDI_{100,peripheral} \right)$$

Finally, with the introduction of helical scanning, a CTDI was developed to take into account the effects of the relative table speed using the pitch factor.<sup>11</sup> This is referred to as  $CTDI_{vol}$  (vol stands for volume) and is defined as:

$$CTDI_{vol} = \frac{CTDI_w}{Pitch}$$

This definition reflects the fact that, with all other factors held constant, the radiation dose will be inversely proportional to pitch. That is, as pitch decreases, the dose will increase linearly by that same amount. This has significant implications for cardiac scanning.

In summary, a series of dose indices have been developed through the years that are unique to CT:

- $CTDI_{FDA}$  represents the measurement across 14 widths of the nominal beam width and hence the measured length varies with the nominal beam width;
- $CTDI_{100}$  represents values measured with a fixed length of the 100 mm pencil ionization chamber, regardless of the nominal beam width;
- $CTDI_w$  is a weighted average of  $CTDI_{100}$  values measured at peripheral and central positions within the cylindrical phantom;
- $CTDI_{vol}$  represents the extension of  $CTDI_w$  that takes into account the table feed or pitch of the actual scan acquisition.

Because it is measured in a cylindrical phantom that is similar to patients only in approximate diameter, these CTDI values are not intended to reflect the actual radiation dose to any specific patient; instead they are just relative indices of the radiation dose. While they may not be very useful for estimating radiation dose to the breast for a specific CT exam, they are very useful in comparing the relative radiation dose of a scan with one set of technical parameters versus another. This is illustrated below.

## 2 KEY TECHNICAL FACTORS IN CT AND THEIR EFFECT ON RADIATION DOSE

In X-ray CT, there are several factors that have a strong effect on the radiation dose. These include the tube current-time product (mAs), beam energy (kilovolt peak or kVp), pitch (or relative table speed) and beam collimation among other factors. These factors and the magnitude of their effect on radiation dose will be described below.

### 2.1 Tube current-time product (mAs)

The tube current-time product is often referred to as the product of tube current (mA) and gantry rotation time (in seconds), or just simply 'mAs.' This term is meant to be proportional to the photon fluence, or total number of photons (regardless of the energy of the photons, which will be discussed in the next section), that are emitted by the x-ray tube.

There are several variations on the term 'mAs.' When the x-ray beam is on for the entire rotation around the patient, then the mAs value just equals the product of the tube current setting in mA and the gantry rotation time. However, as will be described below in section 3, there are times when the beam is not actually on for the entire rotation (such as when a partial scan is performed). In this case, the mAs value will be the product of the tube current setting in mA and the actual beam on time (and *not* the gantry rotation time). Another variation on this term is the term 'effective mAs' or 'mAs/slice'; these terms take into account the pitch value and will be described below in section 2.3.

Radiation dose is directly proportional to this mAs value as it represents the number of photons that are being emitted by the x-ray tube. Therefore, as one increases the mAs, the radiation dose will increase. Similarly, as one decreases the mAs, the radiation dose will decrease. This is illustrated in Table 3.1, in which some  $CTDI_{vol}$  values (defined above) were measured while the mAs value was varied.

### 2.2 Beam energy – kVp

X-ray CT uses an X-ray beam that contains a spectrum of energies. Each spectrum is characterized by the peak

**Table 3.1** Typical radiation dose values measured by  $CTDI_{vol}$  (in mGy) for different mAs settings; all values based on measurements done in 32 cm diameter CTDI phantom for 120 kVp,  $12 \times 1.5$  mm beam collimation, pitch 1.0

mAs	$CTDI_{vol}$
100	7.7 mGy
200	15.4 mGy
300	23.1 mGy
400	30.8 mGy
500	38.5 mGy
600	46.2 mGy

**Table 3.2** Typical radiation dose values measured by  $CTDI_{vol}$  (in mGy) for different kVp settings; all values based on measurements done in 32 cm diameter CTDI phantom for 300 mAs,  $12 \times 1.5$  mm beam collimation, pitch 1.0

kVp	$CTDI_{vol}$
80	7.1 mGy
100	14.3 mGy
120	23.1 mGy
140	35.0 mGy

(or maximum) voltage (kVp) that is applied to the x-ray source. The influence of the kVp setting on radiation dose is illustrated in Table 3.2. This table shows  $CTDI_{vol}$  values measured at different kVp settings. When all other factors (mAs, beam collimation, etc.) are held constant, changing the kVp from 120 to 140 kVp increases the radiation dose by approximately 50%.

## 2.3 Pitch

Pitch is defined for helical scanning as the table travel per rotation divided by the total nominal beam collimation and reflects the relative table speed:

$$\text{Pitch} = \frac{\text{Table Travel per Rotation}}{\text{Total Beam Collimation}}$$

A pitch value of 1.0 represents a contiguous acquisition where the table advances one beam collimation width every rotation. For example, in a 64 slice scanner where the nominal beam collimation might be  $64 \times 0.625$ , the total beam collimation would be 40 mm. If the table travel per rotation were 40 mm, then a pitch of 1.0 would result. If the table travel were faster, say 60 mm per rotation, then a pitch value of 1.5 would result. Often in cardiac scanning, a lower pitch value is used, such as 0.2; this means that the table would only move 8 mm per rotation for that 40 mm nominal beam collimation.

Pitch is accounted for in the  $CTDI_{vol}$  definition. This definition demonstrates that, with all other factors held constant, radiation dose is *inversely* proportional to pitch. That is, the radiation dose for pitch = 2.0 is half of that resulting from using pitch 1.0. Similarly, the radiation dose resulting from using pitch 0.2 is *five times* that resulting from using pitch 1.0. This is shown in Table 3.3.

**Table 3.3** Typical radiation dose values measured by  $CTDI_{vol}$  (in mGy) for different pitch values; all values based on measurements done in 32 cm diameter CTDI phantom for 120 kVp, 300 mAs,  $12 \times 1.5$  mm beam collimation.

Pitch	$CTDI_{vol}$
0.20	115.5 mGy
0.24	96.3 mGy
1.0	23.1 mGy
1.5	15.4 mGy
2.0	11.6 mGy

## 2.4 Beam collimation

In Multidetector row CT (MDCT) scanners, there are often several choices of total nominal beam collimation settings. Note that this refers to the total nominal width of the X-ray beam at the scanner isocenter and *not* the width of the reconstructed slices. A specific example would be for a 64 slice MDCT scanner that has options for beam collimation settings of  $8 \times 0.625$  mm,  $16 \times 0.625$  mm,  $32 \times 0.625$  mm and  $64 \times 0.625$  mm. Each of these would result in a different total nominal beam collimation width at the scanner's isocenter; however, each of these beam collimation settings would allow reconstruction of 0.625 and 1.25 mm thick slices (and perhaps even more slice thicknesses). For MDCT, the actual radiation beam width at isocenter is slightly larger than the nominal beam width; this ensures that all detectors see the same amount of radiation, even the detector rows at the extreme edges. This discrepancy between nominal and actual beam width can have implications on patient dose. Since we are interested in the radiation dose, the radiation dose profile can be measured in air at isocenter and this would describe how close the actual radiation beam width would be to the nominal beam width. Typically for MDCT, when the beam collimation is set to the largest possible width (e.g.  $64 \times 0.625$  mm for a 64 detector row scanner), there is a relatively small difference between the measured beam width and the nominal beam width. However, when the narrowest beam collimation settings are used (e.g.  $8 \times 0.625$  mm setting), the actual beam collimation can be significantly larger than the nominal. This 'overbeaming' can result in significant additional dose. Note that the setting with the least amount of overbeaming is not always the widest setting; for the particular scanner investigated for Table 3.4, the setting with the measured beam width closest to nominal was the 20 mm beam width, not the 40 mm beam width, though the difference

**Table 3.4** Measured beam widths compared to nominal beam collimation settings for a 64 detector row scanner

Nominal beam collimation	Total nominal beam width	Measured beam width	% over nominal
8 × 0.625 mm	5 mm	7.3 mm	46.0%
16 × 0.625 mm	10 mm	11.4 mm	14.0%
32 × 0.625 mm	20 mm	20.3 mm	1.5%
64 × 0.625 mm	40 mm	42.4 mm	6.0%

between these two is not large. These results are described in Table 3.4.

### 3 COMMON CARDIOVASCULAR CT EXAMS AND THEIR RADIATION DOSE

In other chapters within this book, many applications using CT for the cardiovascular system are described. While it is not possible here to describe the radiation dose implications for each one individually, this section will describe a few very common exams and describe the radiation dose that results from each one. The two most common exams of the coronary arteries are a scan for coronary artery calcium and a coronary artery computed tomography angiography (CTA) exam. These two exams are carried out in quite different ways and this has significant implications for radiation dose.

#### 3.1 Prospective ECG-triggered CT – coronary artery calcium scanning

A coronary artery calcium study is often performed on asymptomatic patients and the aim is to assess (and quantify) the amount of calcium present in the coronary arteries. Therefore, this study acquires images just of the coronary arteries with as little motion as possible and, because these are often asymptomatic patients, using as little radiation dose as possible. This means that the examination is done without any intravenous contrast agent and is done using prospective ECG gating in a sequential axial acquisition, although helical scanning techniques are also sometimes used.

In prospective ECG (or cardiac) triggering, the x-ray source is turned on and off so that image projection data is collected only during certain predetermined R-R intervals of the ECG wave (a typical value would be 40% of the

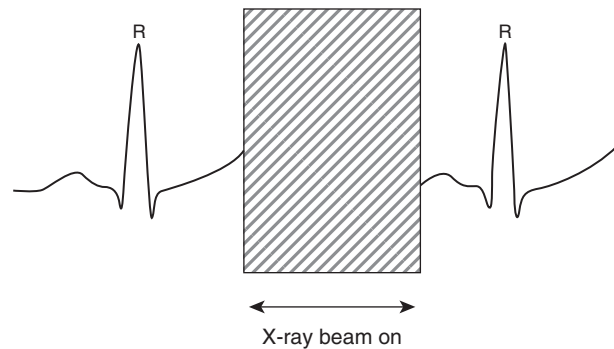


**Figure 3.2.** This figure illustrates that in prospective ECG gating, the x-ray beam is turned on only during the quietest phase of the heart cycle – typically starting at 40% of the R-R interval.

R-R interval, but this has been varied in some studies). In fact, the x-ray source is essentially being triggered (turned on and off) by the ECG wave. This is done so that all of the required projections are acquired during the quietest phases of the ECG cycle to minimize cardiac motion in the resulting image. This is illustrated in Figure 3.2. Note that the arteries are therefore only imaged at one phase of the cardiac cycle, because that is all that is required to quantify the amount of calcium present.

In this exam, the x-ray beam will only be on long enough to create what is known as a ‘partial scan.’ This means that the x-ray beam is on just long enough to collect the minimum amount of data necessary to reconstruct an image; this minimum is 180° of rotation plus the fan angle which typically equals approximately 240° (or 2/3 of a full rotation). For a scanner that can perform a full rotation in 0.5 second, this partial scan time is approximately 0.33 second. For a scanner that can perform a full rotation in 0.33 second, the partial scan time reduces to 0.22 second. Obviously, the shorter the scan acquisition time, the less likely there will be motion while imaging the coronary arteries.

After each exposure, the table will be incremented by the nominal beam width as in conventional contiguous axial (or sequential) scanning. In MDCT scanners, multiple detector rows are used simultaneously to acquire multiple axial images. For example in a 12 × 1.5 mm scan acquisition mode, the nominal beam width is 12 × 1.5 mm, or 9 mm, and the table feed would also be 9 mm to create the contiguous axial scans. In this case, there are 12 separate images, each having 1.5 mm thickness; note that the projection data can also be combined to create six 3 mm thick images (because quantification of coronary artery calcium is typically done on 3 mm thick images). For a 64 detector row scanner, the scan acquisition might be done as a 64 × 0.625 mm scan acquisition with



**Figure 3.3** Image of a CT scan to assess coronary artery calcium; this image shows a calcified plaque in the left anterior descending coronary artery.

a 40 mm table feed and images reconstructed with 2.5 mm thickness. Because these scans are done with contiguous axial scans, this results in the equivalent of a pitch of 1.0.

CT scans to quantify coronary artery calcium are typically done at low mA settings. This is possible because of the higher attenuation values (Hounsfield Units or HU) observed where there is significant calcium in the coronary arteries (Figure 3.3), which are primarily due to calcium's higher atomic

number (and higher k-edge, creating more photoelectric absorption and hence, higher x-ray attenuation).

The radiation dose for these exams is relatively low. This is because they use prospective ECG gating, partial scans, contiguous axial scans and they are performed at low mA settings. Table 3.5 shows some typical technical parameter settings and  $CTDI_{vol}$  values for this kind of exam. These values can be compared to those in previously published works<sup>12-14</sup> for coronary artery exams. These previous estimates of  $CTDI_{vol}$  ranged from 2.2 to 5 mGy and effective dose estimates ranged from 0.6 to 1.6 mSv. These will be compared with other types of exams described in subsequent sections within this chapter.

### 3.2 Retrospective gated CT – coronary angiography scanning

The aim of this examination is to assess whether there is narrowing in any of the coronary arteries. This study is typically performed on patients with symptoms of coronary artery disease and is performed with high resolution imaging in all planes (including thin slices) so that multiplanar reformations and 3D reconstructions can be performed and covering several, if not all, of the phases of the heart cycle, both systole and diastole.

To meet these requirements, and in contrast to the prospective gating done to assess coronary artery calcium, the coronary CT angiogram (CTA) is performed using

**Table 3.5** Radiation dose values estimated from a prospective ECG gated, contiguous axial CT scan typically performed for coronary artery calcium assessment. Note that  $CTDI_{vol}$  values are based on measurement data and that the effective dose and organ doses that follow are based on estimates obtained from the ImPACT CT Dose calculator version  $0.99 \times 15$

<i>Gating used</i>	<i>Prospective ECG</i>	<i>Prospective ECG</i>	<i>Prospective ECG</i>
Number of detector rows	4	16	64
Beam energy in kVp	120	120	120
Beam collimation	4 × 2.5 mm	16 × 1.25 mm	64 × 0.625 mm
Total nominal beam width	10 mm	20 mm	40 mm
Table feed	10 mm	20 mm	40 mm
Rotation time	0.5 sec	0.5 sec	0.33 sec
Partial scan time	0.33 sec	0.33 sec	0.24 sec
(Actual beam on time)			
mA	190	190	264
mAs	63 mAs	63 mAs	63 mAs
$CTDI_{vol}$ (mGy)	6.4	6.2	5.9
Effective dose (mSv)	1.5	1.5	1.3
Breast dose (mGy)	7.1	6.7	6.0
Esophagus dose (mGy)	3.2	3.3	2.9
Thyroid dose (mGy)	0.12	0.12	0.12
Lung dose (mGy)	5.5	5.2	5.0

an injection of an intravenous contrast agent, retrospective ECG gating (described below), and a helical scan with a pitch much less than 1.0. This results in radiation doses that are much higher than in the previous section.

In retrospective ECG gating, the X-ray source is kept on so that image projection data is collected continuously during the helical scan. To ensure that sufficient image projections are acquired for each location at all phases of the ECG wave, the table movement is slowed down significantly by using a low pitch value – typically 0.2 to 0.3. This is done so images can be reconstructed for any phase of the cardiac cycle.

To be able to accurately assess the coronary arteries in any plane, thin slice ( $\leq 2$  mm) acquisitions are performed. With the advent of 16 and 64 slice scanners, these acquisitions are typically done with submillimeter ( $\leq 1$  mm) slice thicknesses. However, when these thinner slices are used, the image noise increases.

These CTA scans are typically done at much higher mA settings than the scans to assess coronary artery calcium. This is true primarily because thin slice images require a higher mA to keep image noise to an acceptable level where the diagnosis can be made with confidence.

Therefore, the radiation dose for CTA exams is higher than for coronary artery calcium scans. This is primarily because this exam uses: (a) retrospective ECG gating which requires low pitch values and (b) thin sections and relatively low image noise, which requires high mAs. Table 3.6 shows some typical technical parameter settings and  $CTDI_{vol}$  values

for this kind of exam. These values can be compared with the values found in references,<sup>12–14</sup> which estimated  $CTDI_{vol}$  to range from 36–55 mGy and effective dose to range from 7–13 mSv for retrospectively gated coronary CTA exams. Please note that these values are significantly higher than the values encountered for the coronary artery calcium scans described in the previous section.

## 4 RECENT ADVANCES IN CT

As multidetector row CT (MDCT) has advanced rapidly in the last several years, there have also been significant developments related to the reduction of radiation dose from MDCT as well.<sup>16</sup> These are discussed in this section along with their strengths and weaknesses in terms of their ability to reduce radiation dose in clinical practice.

### 4.1 Tube current modulation (automatic exposure control for CT)

The purpose of automatic tube current modulation is to maintain constant image quality regardless of patient attenuation characteristics, thus allowing radiation dose to patients to be reduced.<sup>17</sup> That is, rather than using the same tube current through both thick and thin parts of the patient

**Table 3.6** Radiation dose values estimated from a retrospective ECG gated, helical scan with low pitch values performed for coronary artery CT angiography. Note that  $CTDI_{vol}$  values are based on measurement data and that the effective dose and organ doses that follow are based on estimates obtained from the ImPACT CT Dose calculator version 0.99  $\times$  <sup>15</sup>

<i>Gating used</i>	<i>Retrospective ECG</i>	<i>Retrospective ECG</i>	<i>Retrospective ECG</i>
Number of detector rows	4	16	64
Beam energy in kVp	120	120	120
Beam collimation	4 $\times$ 2.5 mm	16 $\times$ 1.25 mm	64 $\times$ 0.625 mm
Reconstructed slice width	2.5 mm	1.25	0.625 mm
Total nominal beam width	10 mm	20 mm	40 mm
Table feed per rotation	2 mm	4.8 mm	9.6 mm
Pitch	0.2	0.24	0.24
Rotation time	0.5 sec	0.5 sec	0.33 sec
mA	250	300	450
mAs	125 mAs	150 mAs	150 mAs
Effective mAs (= mAs/pitch)	625	625	625
$CTDI_{vol}$ (mGy)	63.2	61.9	57.5
Effective dose (mSv)	15	15	13
Breast dose (mGy)	71	67	59
Esophagus dose (mGy)	32	32	29
Thyroid dose (mGy)	1.2	1.2	1.2
Lung dose (mGy)	55	52	49

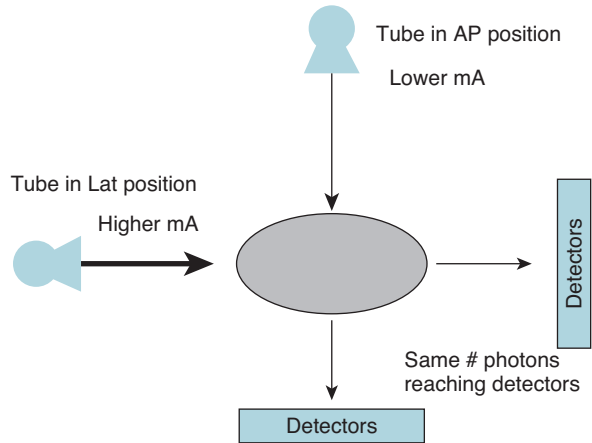


**Figure 3.4** This figure illustrates that for the typical non-circularly shaped patient, the tube current can be varied as the x-ray tube is moved around the patient, resulting in the same number of photons reaching the detectors for each projection angle, which produces a constant noise level while reducing radiation dose.

(such as when the tube moves from an AP position to a lateral position around the patient), the tube current could be reduced when the thinner, less attenuating part of the patient is encountered. This would save radiation dose to the patient and, even though fewer x-ray photons came out of the tube at that position, there would be approximately the same number of photons reaching the detectors because there would be less attenuation through that portion of the body; yielding the same image quality as when a higher number of photons were used in a thicker portion of the body. Thus image quality is maintained, but radiation dose is lowered for that projection through the less attenuating part of the patient. This is illustrated in Figure 3.4.

#### 4.1.1 Conventional tube current modulation methods

There are several kinds of tube current modulation, all of which share this same basic idea.<sup>17–21</sup> The first kind is an angular tube current modulation, where the tube current is only varied with the angle of the x-ray tube current around the patient. This is the kind of tube current modulation referred to in Figure 3.4. In angular (x- and y-axis) tube current modulation, the tube current is varied to equalize the photon flux to the detector as the x-ray tube rotates about the patient (e.g. from the anterior-posterior direction to the lateral direction). Thus, an initial tube current value (or tube current-time product value) is chosen and then the tube

current is modulated (typically, decreased) from that initial value within one gantry rotation. The resulting tube current values might be as shown in Figure 3.4.

The next tube current modulation scheme varies the tube current along the longitudinal (or z-axis) of the patient. In this scheme, the tube current is varied to yield approximately the same image quality across different anatomic regions (e.g. shoulders vs. lung, or abdomen vs. pelvis) despite there being large differences in attenuation. Therefore, the tube current is higher through the more dense/attenuating regions (e.g. shoulders) and then reduced for the lower attenuating regions (e.g. lung). This is illustrated very well in McCollough et al.<sup>17</sup> This can result in substantial dose reduction compared to a constant tube current scheme.

The last of the conventional tube current modulation schemes is a combination where the tube current is modulated in both the angular and longitudinal directions (x, y and z) of the patient, as illustrated in Figure 3.5. This involves variation of the tube current both during gantry rotation and along the z-axis of the patient (i.e., from the anteroposterior direction to the lateral direction, *and* from the shoulders to the abdomen). This comprehensive scheme provides the advantages of both methods above and therefore the dose is adjusted according to the patient-specific attenuation in all three directions.

#### 4.1.2 ECG-gated tube current modulation

In ECG-gated tube current modulation,<sup>22</sup> the tube current is raised and lowered in relation to the ECG wave, rather than based on patient attenuation characteristics as described above. These schemes keep the tube current value high during the portion of the heart cycle where motion is reduced (e.g. diastole) and then reduce the tube current when motion is expected to be high (e.g. systole); this is illustrated in Figure 3.6. In this way, radiation dose can be reduced without incurring much of an image quality penalty as the projections acquired with low mA would typically have significant motion and would not be used. Jakobs et al,<sup>22</sup> reported a mean dose reduction of nearly 50% when this scheme was used.

## 4.2 Dual source CT

In 2006, a dual source CT was introduced by Siemens (Definition, Siemens Medical Solutions, Forchheim, Germany).<sup>23</sup> This unique scanner placed two x-ray

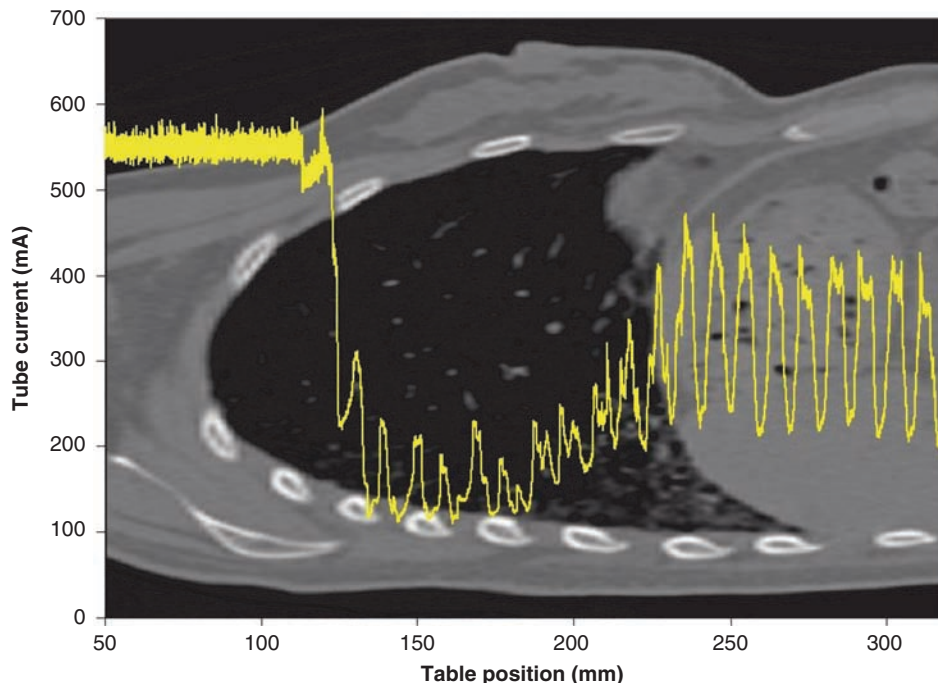


**Figure 3.5** Graph of the tube current (mA) shown with reference to a sagittal plane image of an adult female patient. In this tube current modulation scheme, the tube current is varied both as the tube rotates around the patient (causing the rapid changes in tube current value) and as the tube moves along the longitudinal position of the patient.

sources on the same gantry in the same imaging plane, but offset by  $90^\circ$ ; two separate sets of detectors (similar to that used in the Siemens Sensation 64) are also placed in the same imaging plane, opposite each x-ray source. The primary purpose of this distinctive arrangement was to improve temporal resolution for cardiac imaging. In their article describing system performance,<sup>23</sup> the authors describe a temporal resolution of 83 ms. That is, a complete set of projection data necessary to reconstruct an image was acquired within 83 msec, using single segment reconstruction (temporal resolution improves to an average of 60 msec down to a minimum of 42 msec when dual segment reconstruction methods are used). In addition, because so many projections are acquired simultaneously, this

temporal resolution is maintained for heart rates ranging from 40 bpm all the way up to 120 bpm. This has allowed coronary CT angiogram studies to be performed on patients with a much wider range of heart rates and still yield a successful study with a minimum of cardiac motion in the image.

#### 4.2.2 Dose reduction technologies utilized

While at first glance the notion of two x-ray tubes would suggest a doubling of the radiation dose to the patient for a cardiac CT exam, there have been several dose reduction technologies employed for this scanner. The first is the

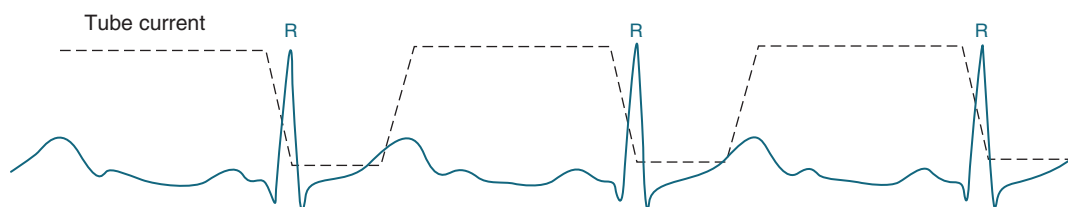


**Figure 3.6** ECG-controlled tube current modulation. The tube current is lowered during phases of ECG wave where cardiac motion is expected to be high, and restored to higher values where cardiac motion is expected to be low.

ECG gated tube current modulation described above. For this scanner, because the amount of time that the x-ray actually has to be on is shorter, the tube current can be reduced for more of the cardiac cycle, thus allowing more dose reduction than in 16 or 64 slice scanners. Another dose reduction technology employed is that, as the heart rate *increases*, the pitch is allowed to increase as well. Therefore, rather than employing a fixed pitch value (typically 0.20 to 0.24) regardless of heart rate, this scanner allows pitch values to range from 0.20 (for heart rates as low as 40 bpm) to 0.40 (for heart rates up to 120 bpm). Thus, not only does this scanner allow imaging at these faster heart rates, the radiation dose is actually decreased at those faster heart rates. While there are other methods employed as well, these two are the primary radiation dose reduction technologies used in this scanner to help keep the radiation dose to levels comparable to previous technologies used for cardiac scanning.

## 5 SUMMARY

CT is being used for a wide variety of cardiac imaging applications, ranging from exams to assess coronary artery calcium to detailed coronary CTA studies of the arteries. In this section, the elements of radiation dose were defined as well as the technical factors that influence dose. The magnitude of radiation dose from several types of CT exams was described as well as some technologies for radiation dose reduction.

As CT technology continues to develop the ability to cover more of the patient with better spatial and temporal resolution, especially if this continues to develop in a cost-effective manner, then its utilization will also increase. Because CT does use ionizing radiation, it is prudent to continue to understand issues related to radiation dose and to encourage methods that will reduce the radiation dose necessary to accomplish the clinical objectives of the imaging study.

## REFERENCES

1. Stern SH, Kaczmarek RV, Spelic DC, Suleiman OH. Nationwide Evaluation of X-ray Trends (NEXT) 2000–2001 survey of patient radiation exposure from computed tomographic (CT) examinations in the United States (abstr). *Radiology* 2001; 221(P): 161.
2. Mollet NR, Cademartiri F, Krestin GP, et al. Improved diagnostic accuracy with 16-row multi-slice computed tomography coronary angiography. *J Am Coll Cardiol*. 2005; 45(1): 128–32.
3. Meijboom WB, Mollet NR, van Mieghem CA, et al. 64-slice Computed Tomography Coronary Angiography in Patients with Non-ST Elevation Acute Coronary Syndrome. *Heart* 2007 (in press).
4. Herzog C, Zangos S, Zwerner P, et al. CT of coronary artery disease. *J Thorac Imaging* 2007 Feb; 22(1): 40–8.
5. Bushberg JT, Seibert JA, Leidholdt EM, Boone JM. The essential physics of medical imaging. 2<sup>nd</sup> ed. Philadelphia, Pa: Lippincott Williams & Wilkins, 2001.
6. International Council on Radiation Protection. 1990 recommendations of the International Commission on Radiological Protection. Publication 60, Annals of the ICRP 1991; 21. Oxford, England: Pergamon, 1991.
7. McCollough CM, Schueler BA. Calculation of effective dose. *Med Phys* 2000; 27: 838–44.
8. McNitt-Gray MF. AAPM/RSNA Physics Tutorial for Residents: Topics in CT. Radiation dose in CT. *Radiographics*. 2002 Nov–Dec; 22(6): 1541–53.
9. Shope TB, Gagne RM, Johnson GC. A method for describing the doses delivered by transmission x-ray computed tomography. *Med Phys* 1991; 8: 488–95.
10. Department of Health and Human Services, Food and Drug Administration. 21 CFR Part 1020: Diagnostic x-ray systems and their major components; amendments to performance standard; Final rule. *Federal Register* 1984, 49, 171.
11. European Guidelines on Quality Criteria for Computed Tomography (EUR 16262 EN, May 1999). Available at: [www.dr.dk/guidelines/ct/quality/index.htm](http://www.dr.dk/guidelines/ct/quality/index.htm). Accessed March 2007.
12. Gerber TC, Kuzo RS, Morin RL. Techniques and parameters for estimating radiation exposure and dose in cardiac computed tomography. *Int J Cardiovasc Imaging* 2005 Feb; 21(1): 165–76.
13. Bae KT, Hong C, Whiting BR. Radiation dose in multidetector row computed tomography cardiac imaging. *J Magn Reson Imaging* 2004 Jun; 19(6): 859–63.
14. Morin RL, Gerber TC, McCollough CH. Radiation dose in computed tomography of the heart. *Circulation* 2003 107(6): 917–22.
15. Imaging Performance Assessment of CT (ImPACT) CT Patient Dosimetry Calculator, version 0.99x. Created 1/20/06. Available at: <http://www.impactscan.org/ctdosimetry.htm>.
16. Linton OW, Mettler FA Jr. National Council on Radiation Protection and Measurements. National conference on dose reduction in CT, with an emphasis on pediatric patients. *Am J Roentgenol*. 2003 Aug; 181(2): 321–9.
17. McCollough CH, Bruesewitz MR, Kofler JM Jr. CT dose reduction and dose management tools: overview of available options. *Radiographics* 2006; 26(2): 503–12.
18. Haaga JR, Miraldi F, MacIntyre W, et al. The effect of mAs variation upon computed tomography image quality as evaluated by in vivo and in vitro studies. *Radiology* 1981; 138: 449–54.
19. Kalra MK, Maher MM, Toth TL, et al. Techniques and applications of automatic tube current modulation for CT. *Radiology* 2004 Dec; 233(3): 649–57.
20. Gies M, Kalender WA, Wolf H, Suess C. Dose reduction in CT by anatomically adapted tube current modulation. I. Simulation studies. *Med Phys* 1999; 26: 2235–47.